



1 The use of QBO, ENSO and NAO perturbations in the 2 evaluation of GOME-2/MetopA total ozone measurements

3 Kostas Eleftheratos^{1,2}, Christos S. Zerefos^{2,3,4,5}, Dimitris S. Balis⁶, Maria-Elissavet Koukoulis⁶,
4 John Kapsomenakis³, Diego G. Loyola⁷, Pieter Valks⁷, Melanie Coldewey-Egbers⁷, Christophe
5 Lerot⁸, Stacey M. Frith⁹, Amund Søvde Haslerud¹⁰, Ivar S. A. Isaksen^{10,11}, Seppo Hassinen¹²

6 ¹Laboratory of Climatology and Atmospheric Environment, Faculty of Geology and Geoenvironment, National and
7 Kapodistrian University of Athens, Greece

8 ²Biomedical Research Foundation of the Academy of Athens, Athens, Greece

9 ³Research Centre for Atmospheric Physics and Climatology, Academy of Athens, Athens, Greece

10 ⁴Mariolopoulos-Kanaginis Foundation for the Environmental Sciences, Athens, Greece

11 ⁵Navarino Environmental Observatory (N.E.O.), Messinia, Greece

12 ⁶Laboratory of Atmospheric Physics, Department of Physics, Aristotle University of Thessaloniki, Greece

13 ⁷Institut für Methodik der Fernerkundung (IMF), Deutsches Zentrum für Luft- und Raumfahrt (DLR),
14 Oberpfaffenhofen, Germany

15 ⁸Royal Belgian Institute for Space Aeronomy (BIRA), Brussels, Belgium

16 ⁹Science Systems and Applications, Inc., Lanham, MD, USA

17 ¹⁰Cicero Center for International Climate Research, Oslo, Norway

18 ¹¹Department of Geosciences, University of Oslo, Oslo, Norway

19 ¹²Finnish Meteorological Institute, Helsinki, Finland

20 *Correspondence to:* Kostas Eleftheratos (kelef@geol.uoa.gr)

21 **Abstract.** In this work we present evidence that quasi cyclical perturbations in total ozone (Quasi Biennial
22 Oscillation (QBO), El Nino Southern Oscillation (ENSO) and North Atlantic Oscillation (NAO)) can be used as
23 independent proxies in validating Global Ozone Monitoring Experiment-2 aboard MetopA (GOME-2A) satellite
24 total ozone data, using ground-based measurements, other satellite data and chemical transport model calculations.
25 The analysis is performed in the frame of the validation strategy on longer time scales within the European
26 Organisation for the Exploitation of Meteorological Satellites (EUMETSAT), Satellite Application Facility on
27 Atmospheric Composition Monitoring (AC SAF) project, and covers the period 2007-2016. In general, we find that
28 GOME-2A total ozone data depict the QBO/ENSO/NAO natural fluctuations in concurrence with co-located Solar
29 Backscatter Ultraviolet Radiometer (SBUV), GOME-type Total Ozone Essential Climate Variable (GTO-ECV) and
30 ground-based (GB) observations. Total ozone from GOME-2A is well correlated with the QBO (highest correlation
31 in the tropics of +0.8) in agreement with SBUV, GTO-ECV and GB data which also give the highest correlation in
32 the tropics. The differences between deseasonalised GOME-2A and GB total ozone in the tropics are within $\pm 1\%$.
33 These differences were tested further as to their correlations with the QBO. The differences had practically no QBO
34 signal, providing an independent test of the stability of the long-term variability of the satellite data. Correlations
35 between GOME-2A total ozone and the Southern Oscillation Index (SOI) were studied over the tropical Pacific
36 Ocean after removing seasonal and QBO related variability. Correlations between ozone and SOI are the order of
37 +0.6, in consistency with SBUV and GB observations. Differences between GOME-2A and GB measurements at
38 the station of Samoa (American Samoa; 14.25° S, 170.6° W) are within $\pm 1.5\%$. We also studied the impact of NAO
39 on total ozone in the northern mid-latitudes in winter. We find very good agreement between GOME-2A and GB



40 observations over Canada and Europe as to their NAO-related variability, with mean differences reaching the $\pm 1\%$
41 levels. The agreement and small differences which were found between the independently produced total ozone data
42 sets as to the influence of QBO, ENSO and NAO show the importance of these climatological proxies as additional
43 tool for monitoring the long-term stability of satellite-ground truth biases.

44 **1 Introduction**

45 Ozone is an important gas of the Earth's atmosphere. In the stratosphere, ozone is considered as *good ozone* because
46 it absorbs ultraviolet-B radiation from the Sun thus it protects the biosphere from a large part of the Sun's harmful
47 radiation (e.g. Eleftheratos et al., 2012; Hegglin et al., 2015). In the lower atmosphere and near the surface, natural
48 ozone has an equally important beneficial role because it initiates the chemical removal of air pollutants from the
49 atmosphere such as carbon monoxide, nitrogen oxides and methane. Above natural levels however, ozone is
50 considered as *bad ozone* because it can harm humans, plants and animals. In addition, increases in tropospheric
51 ozone lead to a warming of the Earth's surface because ozone is a greenhouse gas (Hegglin et al., 2015).

52 Ozone in the atmosphere can be measured by ground-based instruments, by balloons, aircraft and satellites and can
53 be calculated by chemical transport model (CTM) simulations. Measurements by satellites from space provide ozone
54 profiles and column amounts over nearly the entire globe on a daily basis (e.g. WMO, 2014). The three Global
55 Ozone Monitoring Experiment-2 (GOME-2) instruments carried on Metop platforms A, B and C serve this purpose.
56 The first was launched in 2006, the second in 2012 and the last one will be launched in 2018. The three GOME-2
57 instruments will provide unique long-term data sets of more than 15 years (2007-2024) related to atmospheric
58 composition and surface ultraviolet radiation using consistent retrieval techniques (Hassinen et al., 2016). The
59 GOME-2 off-line data is set to make a significant contribution towards climate and atmospheric research while
60 providing near real-time data for use in weather forecasting and air quality forecasting applications (Hassinen et al.,
61 2016).

62 Validation of satellite ozone measurements is performed with ground-based (GB) measurements as well as other
63 satellite instruments (Hassinen et al., 2016). Validation of GOME-2A total ozone for the period 2007-2011 was
64 performed by Loyola et al. (2011) and Koukouli et al. (2012). It was found that GOME-2 total ozone data agree at
65 the $\pm 1\%$ level with GB measurements and other satellite data sets (Hassinen et al., 2016). The consistency between
66 GOME-2A and GOME-2B total ozone columns, including a validation with GB measurements, was presented by
67 Hao et al. (2014). An updated time series of the differences between GOME-2A and GOME-2B with GB
68 observations can be found in Hassinen et al. (2016). The long-term stability of the two satellite instruments was also
69 noted in that study. Both satellites are consistent over the Northern Hemisphere with negligible latitudinal
70 dependence, while over the Southern Hemisphere there is a systematic difference of 1% between the two satellite
71 instruments (Hassinen et al., 2016).

72 Chiou et al. (2014) compared zonal mean total column ozone inferred from three independent multi-year data
73 records, namely, SBUV (v8.6) total ozone, GOME-type Total Ozone Essential Climate Variable (GTO-ECV) and
74 GB total ozone for the period 1996-2011. Their analyses were conducted for the latitudinal zones of 0-30° S, 0-30°



75 N, 50-30° S, and 30-60° N. It was found that, on average, the differences in monthly zonal mean total ozone vary
76 between -0.3 and 0.8% and are well within 1%. In that study it was concluded that despite the differences in the
77 satellite sensors and retrievals methods, the SBUV v8.6 and GTO-ECV data records show very good agreement both
78 in the monthly zonal mean total ozone and the monthly zonal mean anomalies between 60°S and 60°N. The GB
79 zonal means showed larger scatter in the monthly mean data compared to satellite-based records, but the scattering
80 was significantly reduced when seasonal zonal averages were analysed. The differences between SBUV and GB
81 total ozone data presented in Chiou et al. (2014) are well in agreement with Labow et al. (2013), who systematically
82 compared SBUV (v8.6) total ozone data with that measured by Brewer and Dobson instruments at various stations
83 as a function of time, satellite solar zenith angle, and latitude. The comparisons showed good agreement (within
84 $\pm 1\%$) over the past 40 years with very small bias approaching zero over the last decade. Comparisons with ozone
85 sonde data showed good agreement in the integrated column up to 25 hPa with differences not exceeding 5%
86 (Labow et al., 2013).

87 The observed small biases (at the percentage level) between satellite and GB observations of total ozone, as have
88 been documented in the above studies, ensure the provision of accurate satellite ozone measurements. The high
89 accuracy and stability of the satellite instruments is essential for monitoring the expected recovery of the ozone layer
90 resulting from measures adopted by the 1987 Montreal protocol and its amendments (e.g., Zerefos et al., 2009;
91 Loyola et al., 2011). It is known that total ozone varies strongly with latitude and longitude as a result of chemical
92 and transport processes in the atmosphere. Total ozone also varies with season. Seasonal variations are larger over
93 middle and high latitudes and smaller in the tropics (e.g. WMO, 2014). On longer time scales total ozone variability
94 is related to large scale natural oscillations such as the Quasi-Biennial Oscillation (QBO) (e.g. Zerefos et al., 1983;
95 Baldwin et al., 2001), the El Nino Southern Oscillation (ENSO) (e.g. Zerefos et al., 1992; Oman et al., 2013;
96 Coldewey-Egbers et al., 2014), the North Atlantic Oscillation (NAO) (e.g. Ossó et al., 2011; Chehade et al., 2014)
97 and the 11-year solar cycle (e.g. Zerefos et al., 2001; Tourpali et al., 2007; Brönniman et al., 2013). Moreover,
98 volcanic eruptions may also alter the thickness of the ozone layer (Zerefos et al., 1994; Frossard et al., 2013; Rieder
99 et al., 2013; WMO, 2014). These natural perturbations affect the background atmosphere and consequently the
100 distribution of the ozone layer. In this context, the study of the effect of known natural fluctuations in total ozone
101 could serve as additional tool for evaluating the long-term variability of satellite total ozone data records.

102 The objective of the present work is to examine the ability of the GOME-2A total ozone data to capture the
103 variability related to dynamical proxies of global and regional importance such as the QBO, ENSO and NAO, in
104 comparison to GB measurements, other satellite data and model calculations. The variability of total ozone from
105 GOME-2A is compared with the variability of total ozone from the other examined data sets during these naturally-
106 occurring fluctuations. The analysis is performed in the frame of the validation strategy of GOME-2A data on longer
107 time scales within the project of EUMETSAT, AC SAF. The validation includes the study of monthly means of total
108 ozone, the annual cycle of total ozone, the amplitude of the annual cycle [i.e., $(\max - \min)/2$], the relation with the
109 QBO (zonal winds at the equator at 30 hPa), the relation with ENSO (correlation with SOI) and the relation with the
110 NAO (correlations with the NAO index in winter (DJF mean)).



111 The annual cycle describes regular oscillations in total ozone that occur from month to month within a year. In
112 general, month-to-month variations of total ozone are larger in middle and high latitudes than in the tropics. The
113 QBO dominates the variability of the equatorial stratosphere (~16-50 km) and is easily seen as downward
114 propagating easterly and westerly wind regimes, with a variable period averaging approximately 28 months.
115 Circulation changes induced by the QBO affect temperature and chemistry (Baldwin et al., 2001). ENSO and NAO
116 are naturally-occurring patterns or modes of atmospheric and oceanic variability, which orchestrate large variations
117 in climate over large regions with profound impacts on ecosystems (Hurrell and Deser, 2009). We present the level
118 of agreement between satellite-derived GOME-2A and GB total ozone in depicting natural oscillations like QBO,
119 ENSO and NAO, highlighting the importance of these climatological proxies to be used as additional tool for
120 monitoring the long-term stability of satellite-ground truth biases.

121 **2 Data sources**

122 The analysis uses GOME-2 satellite total ozone columns for the period 2007-2016. This data forms part of the
123 operational EUMETSAT AC SAF GOME-2/MetopA GDP4.8 data product provided by the German Aerospace
124 Center (DLR). The GOME-2 total ozone data have been monthly averaged on a $1^{\circ} \times 1^{\circ}$ latitude longitude grid. The
125 overview of the GOME-2A satellite instrument and of the GOME-2 atmospheric data provided by AC SAF can be
126 found in Hassinen et al. (2016).

127 To examine the natural variability of ozone on longer time scales, we have additionally analysed the GOME/ERS-2,
128 SCIAMACHY/Envisat, GOME-2A, and OMI/Aura merged prototype level 3 harmonized data record (GTO-ECV,
129 $1^{\circ} \times 1^{\circ}$) for the period 1995-2016 (Coldewey-Egbers et al., 2015; Garane et al., 2018). This GTO-ECV ozone data
130 product was generated and provided by DLR as part of the European Space Agency Ozone Climate Change
131 Initiative (ESA O3 CCI) project. The ESA O3 CCI merged level-3 record, which is based on
132 GOME/SCIAMACHY/GOME-2A/OMI level-2 data, was obtained using the GODFIT v3.0 retrieval algorithm.
133 More on ESA O3 CCI datasets can be found in the studies by Van Roozendaal et al. (2012), Lerot et al. (2014),
134 Koukouli et al. (2015) and Garane et al. (2018).

135 Both datasets are compared with a combined TOMS/OMI/OMPS satellite total ozone data set constructed using data
136 from the Total Ozone Mapping Spectrometer (TOMS) on Nimbus 7 (1979-1993), TOMS on Meteor 3 (1991-1994),
137 TOMS on Earth Probe (1996-2005), the Ozone Monitoring Instrument (OMI) onboard the NASA Earth Observing
138 System (EOS) Aura satellite (2005-present) and data from the next generation Ozone Mapping Profiler Suite
139 (OMPS) nadir profiler instrument, launched in October 2011 on the Suomi National Polar-orbiting Partnership
140 (NPP) satellite (McPeters et al., 2015). The total ozone data are available at $1^{\circ} \times 1.25^{\circ}$ (TOMS) or $1^{\circ} \times 1^{\circ}$
141 (OMI/OMPS) resolution from <https://acd-ext.gsfc.nasa.gov/anonftp/toms/> (last access: 15 June 2018). From these
142 data we constructed monthly mean total ozone data on a $5^{\circ} \times 5^{\circ}$ grid. To account for known biases between the
143 instruments (e.g., Labow et al., 2013) we use the Solar Backscatter Ultraviolet (SBUV) version 8.6 Merged Ozone
144 Data Set (MOD) monthly zonal mean total ozone (https://acd-ext.gsfc.nasa.gov/Data_services/merged/index.html,
145 also see next paragraph; last access: 15 June 2018) as a reference. We adjust each instrument such that the zonal



146 mean in each 50 band averaged over the instrument lifetime matches the corresponding SBUV MOD zonal mean
147 average. Thus the inherent longitudinal variability is retained from the TOMS/OMI/OMPS measurements but any
148 latitude-dependent bias between the instruments is removed. With the exception of Meteor 3 TOMS in the northern
149 hemisphere, all offsets were within 2% at low and mid-latitudes. Such a data set should not be used for long-term
150 trends but is sufficient for analyzing periodic variability such as QBO, ENSO and NAO. We used data for the period
151 1995-2016.

152 In addition, we compare with satellite SBUV station overpass data from 1995 to 2016. The satellite data are based
153 on measurements from three SBUV-type instruments from April 1970 to the present (continuous data coverage from
154 November 1978). Even though the time series includes different versions of the SBUV instrument, the basic
155 measurement technique remains the same over the advancement of the instrument from the Backscatter Ultraviolet
156 (BUV) to SBUV/2 (Bhartia et al., 2013). Satellite overpass data over various ground-based stations are provided per
157 day from <https://acd-ext.gsfc.nasa.gov/anonftp/toms/sbu/MERGED/> (last access: 15 June 2018). These overpass
158 data are analogous to the SBUV MOD monthly zonal mean data previously mentioned. Both are constructed by first
159 filtering lesser quality measurements and then averaging data from individual satellites when more than one
160 instrument is operating. Monthly averages have been calculated by averaging the daily merged ozone overpass data
161 for stations listed in Supplement Table S1. Details about the data are provided by McPeters et al. (2013) and Frith et
162 al. (2014).

163 We also compare with GB observations of total ozone from a number of stations contributing to the World Ozone
164 and Ultraviolet Radiation Data Centre (WOUDC). The WOUDC data centre is one of six World Data Centres which
165 are part of the Global Atmosphere Watch programme of the World Meteorological Organization (WMO). The
166 WOUDC data centre is operated by the Meteorological Service of Canada, a branch of Environment Canada. In
167 total, we analysed total ozone daily summaries from 193 ground-based stations operating either Brewer, Dobson,
168 filter, SAOZ or microtops instruments. The GB total ozone measurements are available from the website
169 https://woudc.org/archive/Summaries/TotalOzone/Daily_Summary/ (last access: 15 June 2018). The various stations
170 used in this study are listed in Table S1.

171 We have also analysed simulations of total ozone from the global 3-D chemical transport model (CTM) Oslo CTM3
172 (Søvde et al., 2012). The Oslo CTM3 has traditionally been driven by 3-hourly meteorological forecast data from
173 the European Centre for Medium-Range Weather Forecasts (ECMWF) Integrated Forecast System (IFS) model,
174 whereas in this study we apply the OpenIFS model (<https://software.ecmwf.int/wiki/display/OIFS/>) (last access: 15
175 June 2018), cycle 38r1, which is an improvement from Søvde et al. (2012). Details on the model are given in Søvde
176 et al. (2012). The Oslo CTM3 comprises both detailed tropospheric and stratospheric chemistry. Photochemistry is
177 calculated using fast-JX version 6.7c (Prather, 2012), and chemical kinetics from JPL 2010 (Sander et al., 2011).
178 Total ozone columns compare well with measurements and other model studies (Søvde et al., 2012 and references
179 therein). The horizontal resolution of the model is $2.25^\circ \times 2.25^\circ$. We made use of the global monthly mean total
180 ozone columns for the period 1995-2016.



181 To examine the QBO component on total ozone we made use of the monthly mean zonal winds at Singapore at 30
182 hPa. The zonal wind data at 30 hPa were provided by the Freie Universität Berlin (FU-Berlin) at [http://www.geo.fu-](http://www.geo.fu-berlin.de/met/ag/strat/produkte/qbo/qbo.dat)
183 [berlin.de/met/ag/strat/produkte/qbo/qbo.dat](http://www.geo.fu-berlin.de/met/ag/strat/produkte/qbo/qbo.dat) (last access: 15 June 2018) (Naujokat, 1986). The impact of ENSO in
184 the tropics was investigated by using the Southern Oscillation Index (SOI) from the Bureau of Meteorology of the
185 Australian Government (<http://www.bom.gov.au/climate/current/soi2.shtml>) (last access: 15 June 2018). The
186 correlation between total ozone and the NAO index was computed for the winter-mean (DJF) when the NAO
187 amplitude is large (e.g. Hurrell and Deser, 2009), over Canada, Europe and the North Atlantic Ocean. Use was made
188 of the principal component (PC)-based NAO index (DJF) which was provided by the Climate Analysis Section,
189 NCAR, Boulder, USA (available at: [https://climatedataguide.ucar.edu/climate-data/hurrell-north-atlantic-oscillation-](https://climatedataguide.ucar.edu/climate-data/hurrell-north-atlantic-oscillation-nao-index-pc-based)
190 [nao-index-pc-based](https://climatedataguide.ucar.edu/climate-data/hurrell-north-atlantic-oscillation-nao-index-pc-based)) (last access: 15 June 2018). Total ozone variability is also related to dynamical variability for
191 example variability in tropopause height (e.g. Dameris et al., 1995; Hoinka et al., 1996; Steinbrecht et al., 1998).
192 The impact of tropopause variability on total ozone variability was examined by analyzing the tropopause pressure
193 from the independently produced NCEP/NCAR (National Centers for Environmental Prediction/National Center for
194 Atmospheric Research) reanalysis 1 data set computed on a 2.5° grid. The NCEP/NCAR reanalysis data were
195 provided from the web site at <https://www.esrl.noaa.gov/psd/data/gridded/data.ncep.reanalysis.tropopause.html> (last
196 access: 15 June 2018) (Kalnay et al., 1996).

197 **3 Results and discussion**

198 **3.1 Monthly zonal means and annual cycle**

199 Figure 1 compares monthly mean total ozone from GOME-2A and SBUV (v8.6) satellite overpass data for stations
200 shown in Table S1 (Supplement). The GOME-2A data were taken at a spatial resolution of 1°x1° around each of the
201 ground-based monitoring stations listed in Table S1 and then averaged over the tropics, middle and high latitudes of
202 both Hemispheres in 30° latitudinal zones to provide the large scale monthly zonal means for the GOME-2A data.
203 Accordingly, SBUV satellite overpass data were averaged over each geographical zone to provide the large scale
204 zonal means for the SBUV observations. Mean differences and standard deviations between GOME-2A and SBUV
205 total ozone were found to be $+0.1 \pm 0.7\%$ in the tropics (0-30 deg.), about $+0.8 \pm 1.6\%$ in mid-latitudes (30-60 deg.),
206 about $+1.3 \pm 2.2\%$ over the northern high latitudes (60-80 deg. N) and about $-0.5 \pm 2.9\%$ over the southern high
207 latitudes (60-80 deg. S). The differences were estimated as $[\text{GOME-2A} - \text{SBUV}] / \text{SBUV} (\%)$ from January 2007 to
208 December 2016. Small differences were also found between GOME-2A and GB measurements (Figure 2 and Table
209 1), where here GB stations data have been averaged over each geographical zone to provide the large scale zonal
210 means for the GB measurements. Mean differences and standard deviations between GOME-2A and GB total ozone
211 were found to be $-0.7 \pm 1.4\%$ in the tropics (0-30 deg.), $+0.1 \pm 2.1\%$ in mid-latitudes (30-60 deg.), $+2.5 \pm 3.2\%$ over
212 the northern high latitudes (60-80 deg. N) and $0.0 \pm 4.3\%$ over the southern high latitudes (60-80 deg. S). We
213 remind all estimates refer to the period between January 2007 and December 2016.

214 In summary, the largest differences between GOME-2A, SBUV (v8.6) and GB measurements are found over the
215 southern high latitudes. In the tropics and mid-latitudes the respective differences are within $\pm 1\%$ or less, and the



216 results are in line with Chiou et al. (2014). Validation results were also presented by Loyola et al. (2011), Koukouli
217 et al. (2012), Coldewey-Egbers et al. (2015), Koukouli et al. (2015), updates of which are included in Hassinen et al.
218 (2016). Our results based on updated to 2017 data largely confirm those studies, pointing to the good performance of
219 GOME-2A when extending the period of record.

220 Next, we have studied the correlation between total ozone from GOME-2A and SBUV satellite data using linear
221 regression analysis for the period 2007–2016. The regression model showed statistically significant correlations
222 between the different datasets as follows: $R = +0.99$ in the tropics, mid-latitudes and the northern high latitudes and
223 $R = +0.94$ in the southern high latitudes. All correlation coefficients are highly statically significant (99.9%
224 confidence level). In the long-term, statistically significant correlation coefficients ($R \geq +0.94$) are also found
225 between GOME-2A satellite and GB measurements (Figure 2) despite the different type of instruments used to
226 measure total ozone from the ground.

227 A large part of the strong correlations shown in Figures 1 and 2 is attributable to the seasonal variability of total
228 ozone which is presented in Figure 3 for GOME-2A, SBUV and GB data. More specifically, Figure 3 shows the
229 seasonal variations of total ozone from stations mean data averaged per 10 degree latitude zones north and south. At
230 high latitudes our analysis stops at 80 degrees. There is a very good agreement between the annual cycles of total
231 ozone from the three datasets denoting the consistency of the satellite retrievals with GB observations. Similar
232 annual cycles are also found with the GTO-ECV ozone data (not shown). Similar consistency is also revealed for the
233 amplitudes of the annual cycles, computed as $[(\text{maximum value} - \text{minimum value})/2]$ in Dobson Units (DU). Figure
234 4 shows global maps of the amplitude of annual cycle of total ozone for the period 2007-2016 from GOME-2A
235 (upper left panel), GTO-ECV (upper right) and the TOMS/OMI/OMPS (lower left) satellite data. All maps are
236 plotted against the sine of latitude north and south in order to show areas according to their actual size. As can be
237 seen from Figure 4, the amplitude of annual cycle is less than 20 DU in the tropics, increasing as we move towards
238 middle and high latitudes up to 75 DU. Interestingly, there is pattern with small amplitude of annual cycle in the
239 southern mid-latitudes with values of about 10-15 DU, seen in Figure 4 as a blue curved line crossing the longitudes
240 around 60 degrees south, the origin of which is attributed to the small annual variation of total ozone in these parts.
241 These features are consistent between all examined satellite data sets and are reproduced to a large extend by the
242 Oslo CTM3 model as well, except in the southern mid-latitudes where the model seems to underestimate the
243 observed annual cycle (Figure 4 lower right).

244 In summary, we find similar annual cycle and amplitude of annual cycle between total ozone from GOME-2A and
245 the other examined total ozone data sets. The mean differences in the annual cycles of GOME-2A and SBUV
246 satellite data are small in the tropics (0-30 deg.: 0.3 ± 2.4 DU), and increase as we move to mid-latitudes (30-60
247 deg.: 2.4 ± 4.4 DU) and higher latitudes (60-80 deg.: 1.7 ± 4.8 DU). These numbers are consistent with the ones
248 found between GOME-2A and GB measurements (tropics: 1.1 ± 2.3 DU; mid-latitudes: 1.2 ± 5.1 DU; high
249 latitudes: 5.1 ± 7.1 DU). In all latitude zones the correlation coefficients between the annual cycles of GOME-2A –
250 SBUV and GOME-2A – GB data pairs were found to be greater than 0.9.



251 Before examining correlations with the large scale natural fluctuations QBO, ENSO and NAO, the mean annual
252 cycle has been removed from the ozone data sets as described in the next section.

253 3.2 Correlation with QBO

254 We then studied how changes in dynamics affect the ozone columns in the atmosphere. The time series obtained
255 have been deseasonalised by subtracting the long-term monthly mean from each individual monthly mean value.
256 Ozone column variations for different latitude zones in the Northern and Southern Hemispheres have been
257 compared. Figure 5 compares total ozone deseasonalised anomalies (in % of the mean) from GOME-2A and SBUV
258 satellite retrievals in the tropics (10° N– 10° S), sub-tropics (10° – 30°) and mid-latitudes (30° – 60°). The right panel of
259 Figure 5 shows the respective anomalies from GTO-ECV data. Mean differences between GOME-2A and SBUV
260 deseasonalised total ozone data between 60° N and 60° S are less than $\pm 0.5\%$ (Table 2). As can be seen from Table 2
261 and Figure 5, there is a very good agreement between the GOME-2A, GTO-ECV and SBUV total ozone anomalies
262 over the entire period of observations. The correlation coefficients between GOME-2A and SBUV are highly
263 significant everywhere (30° – 60° N: +0.94; 10° – 30° N: +0.95; 10° N– 10° S: +0.98; 10° – 30° S: +0.93; 30° – 60° S:
264 +0.87). The same stands when correlating the GTO-ECV with SBUV deseasonalised data (30° – 60° N: +0.96; 10° –
265 30° N: +0.97; 10° N– 10° S: +0.98; 10° – 30° S: +0.96; 30° – 60° S: +0.93).

266 The line with dots in the middle panel of Figure 5 shows the equatorial zonal winds at 30 hPa which were used as a
267 proxy index to study the impact of QBO on total ozone. The general features include a QBO signal in total ozone at
268 latitudes between 10° N and 10° S which almost matches with the phase of QBO in the zonal winds. At higher
269 northern and southern latitudes there is a clear phase shift in the QBO impact on total ozone. The impact of QBO is
270 most pronounced in the tropics with amplitudes of +4% to –4% and it is less pronounced in the sub-tropics and mid-
271 latitudes. As such, strong positive correlations with the QBO are found in the tropics (correlation between GOME-
272 2A and QBO of about +0.77, t-test = 12.91) and weaker (usually of opposite sign) less significant correlations are
273 found at higher latitudes (about –0.15 in the northern and about –0.45 in the southern extra tropics). Similar strong
274 correlations in the tropics and weaker correlations in the extra tropics with the QBO are found for the GTO-ECV,
275 SBUV and GB data.

276 These features are also evident in Figure 6 which compares GOME-2A (and GTO-ECV) satellite total ozone with
277 GB observations with respect to the QBO. Mean differences and standard deviations between GOME-2A and GB
278 and between GTO-ECV and GB deseasonalised total ozone data do not exceed one percent (Table 2). Again,
279 correlation coefficients between deseasonalised GOME-2A and deseasonalised GB data are highly significant in all
280 latitude zones (30° – 60° N: +0.91; 10° – 30° N: +0.91; 10° N– 10° S: +0.94; 10° – 30° S: +0.87; 30° – 60° S: +0.88). The
281 same stands for the GTO-ECV and GB data pairs (30° – 60° N: +0.94; 10° – 30° N: +0.89; 10° N– 10° S: +0.94; 10° – 30°
282 S: +0.87; 30° – 60° S: +0.85). Our results are in line with Eleftheratos et al. (2013) and Isaksen et al. (2014) who
283 compared QBO-related ozone column variations from the chemical transport model Oslo CTM2 with SBUV
284 satellite data for shorter time periods. In summary, it has been shown that GOME-2A depicts the significant effects
285 of QBO on stratospheric ozone in concurrence with SBUV and GB measurements. The instrument captures
286 correctly the variability of ozone in the tropics and the mid-latitudes, which is nearly in phase with the QBO in the



287 tropics and out of phase in the northern and the southern mid-latitudes as have been shown by earlier studies (e.g.
288 Zerefos, 1983; Baldwin et al., 2001).

289 3.3 Correlation with ENSO

290 Apart from the QBO, which affects the variability of total ozone in the tropics, an important mode of natural climate
291 variability in the tropics is ENSO. To examine the impact of ENSO on total ozone in the tropics we first removed
292 correlations with the QBO and then performed the correlation analysis with the SOI. The effect of the QBO was
293 removed from the time series by using a linear regression model for the total ozone variations at each grid box, of
294 the form:

$$295 \quad D(t) = a_0 + a_1 * QBO(t) + residuals(t); 0 < t \leq T \quad (1)$$

296 where $D(t)$ is the monthly deseasonalised total ozone and t is the time in months with $t=0$ corresponding to the initial
297 month and $t=T$ corresponding to the last month. The term a_0 is the intercept of the statistical model. To model QBO
298 we made use of the equatorial zonal winds at 30 hPa. The term a_1 is the regression coefficient of QBO. The QBO
299 component was removed from the time series by using a phase lag with maximum correlation of 28 months (month
300 lag -14 to month lag 13). Then, the remainders from Eq. (1) have been analysed to study the correlations between
301 total ozone and SOI at each individual grid box.

302 Figure 7 presents the correlations between SOI and total ozone from GOME-2A (upper left panel), GTO-ECV
303 (upper right) and TOMS/OMI/OMPS satellite data (bottom left), as well as between SOI and the Oslo model
304 simulations (bottom right). All four plots refer to the period 2007-2016. As can be seen from Figure 7 (upper left),
305 correlations of >0.3 between GOME-2A total ozone and SOI are found in the tropical Pacific Ocean at latitudes
306 between 25 deg. north and south. These correlations were tested as to their statistical significance in the period
307 2007-2016 and were found to be statistical significant. A similar picture of correlation coefficients is also observed
308 by the GTO-ECV and TOMS/OMI/OMPS data. Both data sets show similar results as to the range of correlations
309 (>0.3) in the tropical Pacific for the common period of observations. Nevertheless, the spatial resolution is higher in
310 the GOME-2A and GTO-ECV (1x1 deg.) data than in the TOMS/OMI/OMPS (5x5 deg.) data, so the former data
311 sets perform better when looking at smaller space scales. We have to note here that in both maps there are larger
312 areas with correlation coefficients >0.3 in the southern part of the tropics than in the northern part. However, this
313 was mostly observed during the period 2007-2016. By examining the longer-term data record of the
314 TOMS/OMI/OMPS data which extend back to the 1979, we find symmetry in the pattern of correlations north and
315 south of the equator in the tropical Pacific Ocean (Figure A1 of Appendix A), which indicates that both sides of the
316 tropical Pacific are affected more or less in a similar way by El Niño/La Niña events. Finally, the Oslo CTM3 gives
317 small correlations (<0.3) in the tropical Pacific Ocean around the equator, except over the northern and southern
318 subtropics where the model compares better with the observations.

319 The small rectangle in Figure 7 corresponds to the South Pacific region (10°-20° S, 180°-220° E) and the blue cross
320 to the station Samoa (American Samoa; 14.25° S, 189.4° E), in which total ozone has been studied as for the impact



321 of ENSO after removing variability related to the annual cycle and the QBO. Figure 8 shows an example of the
322 ENSO impact on total ozone in the South Pacific Ocean. The upper panel shows the time series of total ozone
323 anomalies from GOME-2A, GTO-ECV and TOMS/OMI/OMPS satellite data together with the SOI (Figure 8a).
324 Comparisons of GOME-2A data with GTO-ECV data, SBUV overpass data and GB measurements at the station
325 Samoa are shown in Figure 8b. The dotted line shows the respective tropopause pressure anomalies from NCEP
326 reanalysis. All data sets point to the strong influence of ENSO on total ozone. Most evident is the strong decrease of
327 about 4% in 1997/98 which was caused by the strongest El Niño event in the examined period. A strong decrease is
328 also observed in the tropopause pressures by NCEP. Notable also is the strong La Niña event in 2010 which caused
329 total ozone to increase by about 4%. We calculate a strong correlation between total ozone from GTO-ECV and SOI
330 of +0.62 (99% confidence level), which accounts for about 40% of the variability of total ozone over the tropical
331 Pacific Ocean when the annual cycle and QBO signal are removed. From the regression with SOI we estimated an
332 ENSO-related term from which we calculated the amplitude of ENSO in total ozone as [maximum ozone - minimum
333 ozone]/2. The amplitude of ENSO in total ozone was estimated to be 8.7 DU or 3.4% of the annual mean. This is
334 comparable to the amplitude of annual cycle (7.7 DU or 3.0% of the mean) and ~3 times larger than the amplitude of
335 QBO in this region (2.2 DU or 0.8% of the mean). These results are based on the GTO-ECV total ozone data.
336 Similar results were also found at the station Samoa from GB observations (i.e. correlation with SOI: +0.51,
337 amplitude of ENSO: 7.6 DU or 3.0% of the mean, amplitude of annual cycle: 6.7 DU or 2.7% of the mean).
338 Statistics of total ozone such as mean, amplitude of annual cycle, amplitude of QBO and amplitude of ENSO in total
339 ozone over the selected areas are presented in Table 3. Both satellite, GB and model data show consistent results. It
340 also appears that the station Samoa represents well the greater area in the Southern Pacific as to the impact of
341 ENSO.

342 From Figure 8 it also appears that there are high correlations with the tropopause height. The correlation coefficient
343 between the NCEP tropopause pressure and GOME-2A total ozone over the South Pacific Ocean is of the order of
344 +0.55 (Student's t-test statistics results: t-value = 7.11591, p-value <0.0001, N = 119). Accordingly, the correlation
345 with GTO-ECV ozone data is the order of +0.59 (t-value = 11.67077, p-value <0.0001, N = 259) and with
346 TOMS/OMI/OMPS the order of +0.52 (t-value = 9.49874, p-value <0.0001, N = 241). The high correlation between
347 the tropopause pressure and total ozone on interannual and longer time scales points to the very strong link between
348 these parameters. These links were already documented in the past (e.g. Steinbrecht et al., 1998, 2001) and are
349 verified with the GOME-2A data. At the same time a strong correlation is also evident between tropopause pressure
350 and SOI, again on interannual and longer time scales ($R = +0.66$, t-value = 14.25036, p-value <0.0001, N = 264). The
351 above results point to the strong impact of ENSO on the tropical ozone column through the tropical tropopause;
352 warm (El Niño) and cold (La Niña) events affect the variability of the tropopause which in turn affects the
353 distribution of stratospheric ozone. In the tropics, where total ozone is mainly stratospheric, as the tropopause moves
354 to higher altitudes (lower pressure), the stratosphere is compressed, reducing the amount of stratospheric (total)
355 ozone. This happens during warm (El Niño) episodes. The opposite phenomenon occurs during cold (La Niña)
356 events when the tropopause height decreases (higher pressure) and total ozone is then increased. These events can



357 affect the long-term ozone trends in the tropics when looking at time periods when strong El Niño and La Niña
358 events occur at the beginning and the end of the trend period respectively (Coldewey-Egbers et al., 2014).

359 Furthermore, in Figure 8 we have marked 7 stations in the greater South Asia region (35° - 45° N, 45° - 125° E) where
360 total ozone is anti-correlated with the SOI. Admittedly, these anti-correlations are weak (about -0.3) but we thought
361 worthwhile presenting the time series in these areas as well. Figure 9 shows the variability of total ozone after
362 removing seasonal and QBO related variations, over the South Asia region (upper panel) and over the 7 stations
363 averaged within this region (lower panel). As can be seen from this figure, the explained variance by ENSO is small,
364 not exceeding 9%. In summary, our findings indicate that GOME-2A captures well the disturbances in total ozone
365 during ENSO events with respect to satellite SBUV and GB observations. Our findings on the ENSO-related total
366 ozone variations (low ozone during ENSO warm events, high ozone during ENSO cold events, and magnitude of
367 changes) are in line with recent studies (e.g. Randel and Thompson, 2011; Oman et al., 2013, Sioris et al., 2014)
368 included in the recent Ozone Assessment report (Pawson et al., 2014; WMO, 2014).

369 **3.4 Correlation with NAO**

370 The residuals from Eq. (1), free from seasonal and QBO related variations, were also used to study the correlation
371 between total ozone and NAO in winter (DJF mean). The results are presented in Figure 10 which shows the
372 correlation coefficients between total ozone and NAO index in winter from the GOME-2A (upper left), GTO-ECV
373 (upper right) and TOMS/OMI/OMPS satellite data (lower left), and the Oslo CTM3 model calculations (lower
374 right). Negative correlations between total ozone and NAO are presented with blue colours while positive
375 correlations with red colours. From Figure 10 (upper left) it appears that total ozone is strongly correlated with NAO
376 in many regions. Strong negative correlation coefficients are observed in the majority of the northern mid-latitudes
377 (R about -0.6) while positive correlations exist in the tropics and some negative correlations in the southern mid-
378 latitudes. These characteristics are observed in both GTO-ECV and TOMS/OMI/OMPS datasets and are reproduced
379 by the Oslo model as well, all for the common period 2008-2016.

380 We note here that the results of the correlation analysis for the period 2008-2016 were based on a small sample of
381 data (9 winters as DJF means) and therefore many of these correlation coefficients may not be statistically
382 significant. The statistical significance of the correlation coefficients in every grid box was tested only with the
383 TOMS/OMI/OMPS data (Figure A2, Appendix A), which provided us the opportunity to calculate the respective
384 correlations using more data (37 winter means). It appears that when extending the data back to the 1980's the
385 negative correlations in the southern mid-latitudes disappear while the positive correlations in the tropics become
386 weaker; yet the observed anti-correlation between total ozone and NAO index in the northern mid-latitude zone
387 holds strong. The dotted line in the plot shows areas with statistically significant correlation coefficients (99%
388 confidence level). Indeed, statistically significant correlations between total ozone and NAO index in the long-term
389 are found only over the northern mid-latitudes and not elsewhere.

390 According to this finding we have restricted the analysis of NAO to the northern mid-latitudes. Rectangles (Figure
391 10, upper left) correspond to two regions in the North Atlantic, i.e., 35° - 50° N, 20° - 50° W and 15° - 27° N, 30° - 60° W



392 respectively, which were studied for the impact of NAO on total ozone after removing variability related to the
393 annual cycle and the QBO. In addition we have studied a number of stations in Canada, USA, and Europe
394 contributing ozone data to WOUDC, which are marked by red and green crosses in Figure 10. The red crosses refer
395 to the monitoring stations in Canada and the US, and the green crosses to the stations in Europe. In Figure 11 we
396 present the times series of total ozone anomalies from GOME-2A, GTO-ECV and TOMS/OMI/OMPS satellite data
397 along with the NAO index in winter over the North Atlantic. Model calculations are shown as well. The dotted line
398 shows the respective tropopause pressure anomalies from NCEP reanalysis. Comparisons between GOME-2A,
399 GTO-ECV, SBUV (v8.6) overpass data and GB measurements over the various stations in Canada, USA and Europe
400 are shown in Figure 12.

401 The observed anomalies over the North Atlantic Ocean point to the strong influence of NAO on total ozone in
402 winter. Most evident is the strong increase in total ozone in 2010 of more than 8% particularly over 35°-50° N and
403 20°-50° W. This increase was accompanied by a strong increase in tropopause pressures. Both changes (in total
404 ozone and tropopause pressures) occurred under a strong negative phase of NAO, the strongest one in the past 20
405 years. We observe strong anti-correlations among total ozone and NAO index in winter ($R = -0.72$ over 35°-50° N,
406 20°-50° W), which is statistically significant at the 99% confidence level. This anti-correlation suggests that about
407 50% of the variability of total ozone in winter is explained by NAO when the annual cycle and QBO signal are
408 removed. From the regression with the NAO index we derived a NAO-related term from which we calculated the
409 amplitude of NAO in total ozone as [maximum ozone - minimum ozone]/2. The amplitude of NAO over the North
410 Atlantic region (35°-50° N, 20°-50° W) was estimated to be about 18 DU or 5.8% of the annual mean. This is about
411 half of the amplitude of the annual cycle (which is ~37 DU or 11.7% of the mean). Similar correlation and
412 amplitude were also found with the combined TOMS/OMI/OMPS satellite data and the Oslo CTM3 model
413 simulations.

414 A similar but opposite correlation is found over the southern part of the North Atlantic (15°-27° N, 30°-60° W).
415 Here, we estimate a significant correlation coefficient with NAO of +0.69, amplitude of NAO of about 9 DU (3.2%
416 of the annual mean) and amplitude of annual cycle of about 16 DU (5.7% of the mean). Again, similar estimates are
417 found with the TOMS/OMI/OMPS satellite data and reproduced by the model calculations as well. The annual mean
418 total ozone and the amplitudes of annual cycle, QBO and NAO in total ozone over the studied regions in the North
419 Atlantic are summarised in Table 4.

420 The time series of total ozone anomalies and of the NAO index for the examined stations in Canada, USA and
421 Europe are presented in Figure 12. Table 5 presents the respective statistics. The correlation between total ozone and
422 the NAO index in winter after removing from ozone variability related to the annual cycle and the QBO is -0.44
423 (95% confidence level). Again, a particular feature was the total ozone increase in 2010 by 6% of the mean
424 associated with the negative NAO phase. Noteworthy on this increase is the consistency with the GB measurements
425 and the satellite SBUV overpassing data, and in general the agreement found between the variability of the
426 tropopause pressures and total ozone. Table 5 indicates that in Canada and USA, the amplitude of NAO in total



427 ozone in winter is about 10 DU (or 3% of the mean), while it is higher over Europe estimated to be about 16 DU (or
428 5% of the mean).

429 In summary, our findings based on GOME-2A, GTO-ECV and SBUV overpass data are in line with those found by
430 Ossó et al. (2011) and Steinbrecht et al. (2011) who analysed TOMS and OMI satellite data, and GB measurements
431 at the station Hohenpeissenberg, respectively. During winter, total ozone variability associated with the NAO is
432 particularly important over northern Europe, the U.S. East Coast, and Canada, explaining up to 30% in total ozone
433 variance for this region (Ossó et al., 2011). Also, both studies found unusually high total ozone columns in 2010
434 over much of the Northern Hemisphere and related them to the negative phase of NAO or AO (the Arctic
435 Oscillation).

436 4 Conclusions

437 We have studied the ability of GOME-2/MetopA (GOME-2A) satellite total ozone retrievals to capture known
438 natural oscillations such as the QBO, ENSO and NAO. In general, GOME-2A depicts these natural oscillations in
439 concurrence with GTO-ECV, TOMS/OMI/OMPS, SBUV (v8.6) satellite overpass data, ground-based
440 measurements (Brewer, Dobson, filter and SAOZ) and chemical transport model calculations (Oslo CTM3).

441 Mean differences between GOME-2A and SBUV total ozone were found to be $+0.1 \pm 0.7\%$ in the tropics (0-30
442 deg.), about $+0.8 \pm 1.6\%$ in mid-latitudes (30-60 deg.), about $+1.3 \pm 2.2\%$ over the northern high latitudes (60-80
443 deg. N) and about $-0.5 \pm 2.9\%$ over the southern high latitudes (60-80 deg. S). These differences were estimated as
444 $[\text{GOME-2A} - \text{SBUV}] / \text{SBUV} (\%)$ from January 2007 to December 2016. Small differences were also found
445 between GOME-2A and GB measurements, with standard deviations of the differences being $\pm 1.4\%$ in the tropics,
446 $\pm 2.1\%$ in mid-latitudes, and $\pm 3.2\%$ and $\pm 4.3\%$ over the northern and the southern high latitudes respectively.

447 The variability of total ozone from GOME-2A has been compared with the variability of total ozone from other
448 examined data sets as to their agreement to depict natural atmospheric phenomena such as the QBO, ENSO and
449 NAO. First, we studied correlations between total ozone and the QBO after removing from the ozone data sets
450 variability related to the seasonal cycle. Then, we examined correlations between total ozone, ENSO and NAO, after
451 removing variability related to the QBO. Our main results are as follows:

452 **QBO:** Total ozone from GOME-2A is well correlated with the Quasi-Biennial Oscillation ($+0.8$ in the tropics) in
453 agreement with GTO-ECV, SBUV and GB data. The amplitude of QBO on total ozone maximizes around the
454 equator and it is estimated to about 4% of the mean. Going from low to mid-latitudes there is a clear phase shift in
455 the QBO impact on total ozone. Correlation coefficients between GOME-2A total ozone and the QBO over 30-60
456 deg. north and south are -0.1 and -0.5 respectively, in agreement with the correlations between GB total ozone and
457 the QBO (-0.2 and -0.5 , accordingly).

458 **ENSO:** Correlation coefficients among GOME-2A total ozone and SOI in the tropical Pacific Ocean are estimated
459 to be about $+0.6$, consistent with GTO-ECV, SBUV and GB observations. It was found that the ENSO signal is
460 evident and consistent in all examined datasets. The amplitude of the El Nino Southern Oscillation in total ozone is



461 about 6–9 DU corresponding to about 2.5–3.5% of the annual mean. Differences between GOME-2A, GTO-ECV
462 and GB measurements during warm (El Niño) and cold (La Niña) events are within $\pm 1.5\%$.

463 **NAO:** The respective results as far as the impact of North Atlantic Oscillation over the northern mid-latitudes
464 showed a clear NAO signal in winter in all data sets, with amplitudes of about 17–20 DU (about 5–6% of the annual
465 mean). Comparison with GB observations over Canada and Europe showed very good agreement between GOME-
466 2A, GTO-ECV and GB observations as to the influence by NAO, with differences within $\pm 1\%$.

467 Additionally to the usual validation methods, which compare monthly mean and zonal mean total ozone data and
468 analyse the differences between satellite and GB instruments, we showed here that quasi cyclical perturbations such
469 as the QBO, ENSO and NAO can serve as independent proxies of spatiotemporal variation in validating GOME-2A
470 satellite total ozone against ground-based and other satellite total ozone data sets. The agreement and small
471 differences which were found between the variability of total ozone from GOME-2A and the variability of total
472 ozone from other satellite retrievals and ground-based measurements during these naturally-occurring oscillations
473 verify the good quality of GOME-2A satellite total ozone to be used in ozone-climate research studies.

474 **Data availability**

475 Satellite SBUV (v8.6) total ozone station overpass data were downloaded from [https://acd-](https://acd-ext.gsfc.nasa.gov/Data_services/merged/index.html)
476 [ext.gsfc.nasa.gov/Data_services/merged/index.html](https://acd-ext.gsfc.nasa.gov/Data_services/merged/index.html) (last access: 15 June 2018) (McPeters et al., 2013; Bhartia et al.,
477 2013). GTO-ECV total ozone data are available at <http://www.esa-ozone-cci.org/?q=node/160> (last access: 15 June
478 2018) (Coldewey-Egbers et al., 2015; Garane et al., 2018). Ground-based total ozone daily summaries were obtained
479 from the World Ozone and UV Data Centre (WOUDC) at
480 https://woudc.org/archive/Summaries/TotalOzone/Daily_Summary/ (last access: 15 June 2018). The QBO
481 component on total ozone was examined by using the monthly mean zonal winds at Singapore at 30 hPa. Zonal
482 wind data at 30 hPa were provided by the Freie Universität Berlin (FU-Berlin) at [http://www.geo.fu-](http://www.geo.fu-berlin.de/met/ag/strat/produkte/qbo/qbo.dat)
483 [berlin.de/met/ag/strat/produkte/qbo/qbo.dat](http://www.geo.fu-berlin.de/met/ag/strat/produkte/qbo/qbo.dat) (last access: 15 June 2018) (Naujokat, 1986). The Southern Oscillation
484 Index (SOI) was provided by the Bureau of Meteorology of the Australian Government at
485 <http://www.bom.gov.au/climate/current/soi2.shtml> (Australian Government – Bureau of Meteorology, 2018). The
486 NAO index for December, January and February was provided by the Climate Analysis Section, NCAR, Boulder,
487 USA at <https://climatedataguide.ucar.edu/climate-data/hurrell-north-atlantic-oscillation-nao-index-pc-based> (last
488 access: 15 June 2018) (Hurrell and Deser, 2009). The tropopause pressures from the NCEP/NCAR reanalysis 1 data
489 set were downloaded from <https://www.esrl.noaa.gov/psd/data/gridded/data.ncep.reanalysis.tropopause.html> (last
490 access: 15 June 2018) (Kalnay et al., 1996).

491 **Competing interests**

492 The authors declare that they have no conflict of interest.



493 Acknowledgements

494 Development of the GOME-2/MetopA total ozone products and their validation has been funded by the AC SAF
495 project with EUMETSAT and national contributions. We further acknowledge the Mariolopoulos-Kanaginis
496 Foundation for the Environmental Sciences, the ESA Ozone CCI project and the NASA Goddard Space Flight
497 Centre. The ground-based data used in this publication were obtained as part of WMO's Global Atmosphere Watch
498 (GAW) and are publicly available via the World Ozone and UV Data Centre (WOUDC). The authors would like to
499 thank all the investigators that provide quality assured total ozone column data on a timely basis to the WOUDC
500 database. KE and CS would like to dedicate the study to the memory of Professor Ivar Isaksen (University of Oslo)
501 who passed away on May 16th, 2017.

502 References

- 503 Australian Government – Bureau of Meteorology: Southern Oscillation Index (SOI) since 1986, available at
504 <http://www.bom.gov.au/climate/current/soi2.shtml>, last access: 15 June 2018.
- 505 Baldwin, M. P., Gray, L. J., Dunkerton, T. J., Hamilton, K., Haynes, P. H., Randel, W. J., Holton, J. R., Alexander,
506 M. J., Hirota, I., Horinouchi, T., Jones, D. B. A., Kinnersley, J. S., Marquardt, C., Sato, K., and Takahashi, M.: The
507 quasi-biennial oscillation, *Rev. Geophys.*, 39, 179-229, doi: 10.1029/1999RG000073, 2001.
- 508 Bhartia, P. K., McPeters, R. D., Flynn, L. E., Taylor, S., Kramarova, N. A., Frith, S., Fisher, B., and DeLand, M.:
509 Solar Backscatter UV (SBUV) total ozone and profile algorithm, *Atmos. Meas. Tech.*, 6, 2533–2548, doi:
510 10.5194/amt-6-2533-2013, 2013.
- 511 Brönnimann, S., Bhend, J., Franke, J., Flückiger, S., Fischer, A. M., Bleisch, R., Bodeker, G., Hassler, B., Rozanov,
512 E., and Schraner, M.: A global historical ozone data set and prominent features of stratospheric variability prior to
513 1979, *Atmos. Chem. Phys.*, 13 (18), 9623-9639, doi: 10.5194/acp-13-9623-2013, 2013.
- 514 Chehade, W., Weber, M., and Burrows, J. P.: Total ozone trends and variability during 1979-2012 from merged data
515 sets of various satellites, *Atmos. Chem. Phys.*, 14, 7059–7074, doi: 10.5194/acp-14-7059-2014, 2014.
- 516 Chiou, E. W., Bhartia, P. K., McPeters, R. D., Loyola, D. G., Coldewey-Egbers, M., Fioletov, V. E., Van
517 Roozendaal, M., Spurr, R., Lerot, C., and Frith, S. M.: Comparison of profile total ozone from SBUV (v8.6) with
518 GOME-type and ground-based total ozone for a 16-year period (1996 to 2011), *Atmos. Meas. Tech.*, 7, 1681–1692,
519 doi: 10.5194/amt-7-1681-2014, 2014.
- 520 Coldewey-Egbers, M., Loyola R., D. G., Braesicke, P., Dameris, M., van Roozendaal, M., Lerot, C., and W.
521 Zimmer, W.: A new health check of the ozone layer at global and regional scales, *Geophys. Res. Lett.*, 41, 4363–
522 4372, doi:10.1002/2014GL060212, 2014.
- 523 Coldewey-Egbers, M., Loyola, D. G., Koukouli, M., Balis, D., Lambert, J.-C., Verhoelst, T., Granville, J., van
524 Roozendaal, M., Lerot, C., Spurr, R., Frith, S. M., and Zehner, C.: The GOME-type Total Ozone Essential Climate



- 525 Variable (GTO-ECV) data record from the ESA Climate Change Initiative, Atmos. Meas. Tech., 8, 3923–3940, doi:
526 10.5194/amt-8-3923-2015, 2015.
- 527 Dameris, M., Nodorp, D., and Sausen, R.: Correlation between Tropopause Height Pressure and TOMS-Data for the
528 EASOE-Winter 1991/1992, Beitr. Phys. Atmosph., 68 (3), 227-232, 1995.
- 529 Eleftheratos, K., Isaksen, I., Zerefos, C., Nastos, P., Tourpali, K., and Rognerud, B.: Ozone variations derived by a
530 chemical transport model, Water, Air and Soil Pollution, 224:1585, doi: 10.1007/s11270-013-1585-2, 2013.
- 531 Eleftheratos, K., Isaksen, I. S. A., Zerefos, C. S., Tourpali, K., and Nastos, P.: Comparison of Ozone Variations from
532 Model Calculations (OsloCTM2) and Satellite Retrievals (SBUV), 11th International Conference on Meteorology,
533 Climatology and Atmospheric Physics (COMECAP 2012), Athens, Greece, 29 May – 1 June 2012, C. G. Helmis
534 and P. T. Nastos (eds.), Advances in Meteorology, Climatology and Atmospheric Physics, Springer Atmospheric
535 Sciences, DOI 10.1007/978-3-642-29172-2_132, © Springer-Verlag Berlin Heidelberg, pp. 945–950, 2012.
- 536 Frith, S. M., Kramarova, N. A., Stolarski, R. S., McPeters, R. D., Bhartia, P. K., and Labow, G. J.: Recent changes
537 in total column ozone based on the SBUV Version 8.6 merged ozone data set, J. Geophys. Res., 119, 9735–9751,
538 doi: 10.1002/2014JD021889, 2014.
- 539 Frossard, L., Rieder, H. E., Ribatet, M., Staehelin, J., Maeder, J. A., Di Rocco, S., Davison, A. C., and Peter, T.: On
540 the relationship between total ozone and atmospheric dynamics and chemistry at mid-latitudes – Part 1: Statistical
541 models and spatial fingerprints of atmospheric dynamics and chemistry, Atmos. Chem. Phys., 13 (1), 147-164, doi:
542 10.5194/acp-13-147-2013, 2013.
- 543 Garane, K., Lerot, C., Coldewey-Egbers, M., Verhoelst, T., Koukouli, M. E., Zyrichidou, I., Balis, D. S., Danckaert,
544 T., Goutail, F., Granville, J., Hubert, D., Keppens, A., Lambert, J.-C., Loyola, D., Pommereau, J.-P., Van
545 Roozendael, M., and Zehner, C.: Quality assessment of the Ozone_cci Climate Research Data Package (release
546 2017) – Part 1: Ground-based validation of total ozone column data products, Atmos. Meas. Tech., 11, 1385-1402,
547 doi:10.5194/amt-11-1385-2018, 2018.
- 548 Hao, N., Koukouli, M. E., Inness, A., Valks, P., Loyola, D. G., Zimmer, W., Balis, D. S., Zyrichidou, I., Van
549 Roozendael, M., Lerot, C., and Spurr, R. J. D.: GOME-2 total ozone columns from MetOp-A/MetOp-B and
550 assimilation in the MACC system, Atmos. Meas. Tech., 7, 2937–2951, doi: 10.5194/amt-7-2937-2014, 2014.
- 551 Hassinen, S., Balis, D., Bauer, H., Begoin, M., Delcloo, A., Eleftheratos, K., Gimeno Garcia, S., Granville, J.,
552 Grossi, M., Hao, N., Hedelt, P., Hendrick, F., Hess, M., Heue, K.-P., Hovila, J., Jönch-Sørensen, H., Kalakoski, N.,
553 Kauppi, A., Kiemle, S., Kins, L., Koukouli, M. E., Kujanpää, J., Lambert, J.-C., Lang, R., Lerot, C., Loyola, D.,
554 Pedernana, M., Pinardi, G., Romahn, F., van Roozendael, M., Lutz, R., De Smedt, I., Stammes, P., Steinbrecht, W.,
555 Tamminen, J., Theys, N., Tilstra, L. G., Tuinder, O. N. E., Valks, P., Zerefos, C., Zimmer, W., and Zyrichidou, I.:
556 Overview of the O3M SAF GOME-2 operational atmospheric composition and UV radiation data products and data
557 availability, Atmos. Meas. Tech., 9, 383–407, doi: 10.5194/amt-9-383-2016, 2016.



- 558 Hegglin, M. I., Fahey, D. W., McFarland, M., Montzka, S. A., and Nash, E. R.: Twenty questions and answers about
559 the ozone layer: 2014 update, *Scientific Assessment of Ozone Depletion: 2014*, 84 pp., World Meteorological
560 Organization, Geneva, Switzerland, ISBN: 978-9966-076-02-1, 2015.
- 561 Hoinka, K. P., Claude, H., and Köhler, U.: On the correlation between tropopause pressure and ozone above Central
562 Europe, *Geophys. Res. Lett.*, 23 (14), 1753-1756, 1996.
- 563 Hurrell, J. W., and Deser, C.: North Atlantic climate variability: The role of the North Atlantic Oscillation, *Journal*
564 *of Marine Systems*, 78, 28-41, doi: 10.1016/j.jmarsys.2008.11.026, 2009.
- 565 Isaksen, I. S. A., Berntsen, T. K., Dalsøren, S. B., Eleftheratos, K., Orsolini, Y., Rognerud, B., Stordal, F., Søvde, O.
566 A., Zerefos, C., and Holmes, C. D.: Atmospheric ozone and methane in a changing climate, *Atmosphere*, 5, 518–
567 535, doi: 10.3390/atmos5030518, 2014.
- 568 Kalnay, E., Kanamitsu, M., Kistler, R., Collins, W., Deaven, D., Gandin, L., Iredell, M., Saha, S., White, G.,
569 Woollen, J., Zhu, Y., Chelliah, M., Ebisuzaki, W., Higgins, W., Janowiak, J., Mo, K. C., Ropelewski, C., Wang, J.,
570 Leetmaa, A., Reynolds, R., Jenne, R., and Joseph, D.: The NCEP/NCAR 40-year reanalysis project, *Bulletin of the*
571 *American Meteorological Society*, Vol. 77, No. 3, 437-472, 1996.
- 572 Koukouli, M. E., Balis, D. S., Loyola, D., Valks, P., Zimmer, W., Hao, N., Lambert, J.-C., Van Roozendael, M.,
573 Lerot, C., and Spurr, R. J. D.: Geophysical validation and long-term consistency between GOME-2/MetOp-A total
574 ozone column and measurements from the sensors GOME/ERS-2, SCIAMACHY/ENVISAT and OMI/Aura,
575 *Atmos. Meas. Tech.*, 5, 2169–2181, doi: 10.5194/amt-5-2169-2012, 2012.
- 576 Koukouli, M. E., Lerot, C., Granville, J., Goutail, F., Lambert, J.-C., Pommereau, J.-P., Balis, D., Zyrichidou, I., Van
577 Roozendael, M., Coldewey-Egbers, M., Loyola, D., Labow, G., Frith, S., Spurr, R., Zehner, C.: Evaluating a new
578 homogeneous total ozone climate data record from GOME/ERS-2, SCIAMACHY/Envisat and GOME-2/MetOp-A,
579 *J. Geophys. Res. Atmos.*, 120, doi: 10.1002/2015JD023699, 2015.
- 580 Labow, G. J., McPeters, R. D., Bhartia, P. K., and Kramarova, N.: A comparison of 40 years of SBUV
581 measurements of column ozone with data from the Dobson/Brewer network, *J. Geophys. Res. Atmos.*, 118, 7370–
582 7378, doi:10.1002/jgrd.50503, 2013.
- 583 Lerot, C., Van Roozendael, M., Spurr, R., Loyola, D., Coldewey-Egbers, M., Kochenova, S., van Gent, J., Koukouli,
584 M., Balis, D., Lambert, J.-C., Granville, J., and Zehner, C.: Homogenized total ozone data records from the
585 European sensors GOME/ERS-2, SCIAMACHY/Envisat, and GOME-2/MetOp-A, *J. Geophys. Res. Atmos.*, 119,
586 1639–1662, doi: 10.1002/2013JD020831, 2014.
- 587 Loyola, D. G., Koukouli, M. E., Valks, P., Balis, D. S., Hao, N., Van Roozendael, M., Spurr, R. J. D., Zimmer, W.,
588 Kiemle, S., Lerot, C., and Lambert, J.-C.: The GOME-2 total column ozone product: retrieval algorithm and ground-
589 based validation, *J. Geophys. Res.*, 116, D07302, doi: 10.1029/2010JD014675, 2011.
- 590 McPeters, R. D., Bhartia, P. K., Haffner, D., Labow, G. J., and Flynn, L.: The version 8.6 SBUV ozone data record:
591 An overview, *J. Geophys. Res.*, 118, 8032–8039, doi: 10.1002/jgrd.50597, 2013.



- 592 McPeters, R. D., Frith, S., and Labow, G. J.: OMI total column ozone: extending the long-term data record, Atmos.
593 Meas. Tech., 8, 4845-4850, [soi:10.5194/amt-8-4845-2015](https://doi.org/10.5194/amt-8-4845-2015), 2015.
- 594 Naujokat, B., 1986: An update of the observed quasi-biennial oscillation of the stratospheric winds over the tropics,
595 J. Atmos. Sci., 43, 1873-1877.
- 596 Oman, L., Douglass, A., Ziemke, J., Rodriguez, J., Waugh, D., and Nielsen, J.: The ozone response to ENSO in
597 Aura satellite measurements and a chemistry-climate simulation, J. Geophys. Res., 118 (2), 965-976, [doi:](https://doi.org/10.1029/2012JD018546)
598 10.1029/2012JD018546, 2013.
- 599 Ossó, A., Sola, Y., Bech, J., and Lorente, J.: Evidence for the influence of the North Atlantic Oscillation on the total
600 ozone column at northern low latitudes and midlatitudes during winter and summer seasons, J. Geophys. Res., 116
601 (D24), D24122, [doi: 10.1029/2011JD016539](https://doi.org/10.1029/2011JD016539), 2011.
- 602 Pawson, S., and Steinbrecht, W. (Lead Authors), Charlton-Perez, A. J., Fujiwara, M., Karpechko, A. Yu.,
603 Petropavlovskikh, I., Urban, J., and Weber, M.: Update on global ozone: Past, present, and future, V. E. Violeto
604 and U. Langematz (Eds), Chapter 2 in Scientific Assessment of Ozone Depletion: 2014, Global Ozone Research and
605 Monitoring Project – Report No. 55, World Meteorological Organization, Geneva, Switzerland, 2014.
- 606 Prather, M.: Fast-JX version 6.7c, available at: <ftp://halo.ess.uci.edu/public/prather/Fast-J/> (last access: 15 June
607 2018), 2012.
- 608 Randel, W. J., and Thompson, A. M.: Interannual variability and trends in tropical ozone derived from SAGE II
609 satellite data and SHADOZ ozonesondes, J. Geophys. Res., 116 (D7), D07303, [doi: 10.1029/2010JD015195](https://doi.org/10.1029/2010JD015195), 2011.
- 610 Rieder, H. E., Frossard, L., Ribatet, M., Staehelin, J., Maeder, J. A., Di Rocco, S., Davison, A. C., Peter, T., Weihs,
611 P., and Holawe, F.: On the relationship between total ozone and atmospheric dynamics and chemistry at
612 midlatitudes – Part 2: The effects of the El Niño/Southern Oscillation, volcanic eruptions and contributions of
613 atmospheric dynamics and chemistry to long-term total ozone changes, Atmos. Chem. Phys., 13 (1), 165-179, [doi:](https://doi.org/10.5194/acp-13-165-2013)
614 10.5194/acp-13-165-2013, 2013.
- 615 Sander, S. P., Abbatt, J., Barker, J. R., Burkholder, J. B., Friedl, R. R., Golden, D. M., Huie, R. E., Kolb, C. E.,
616 Kurylo, M. J., Moortgat, G. K., Orkin V. L., and Wine, P. H.: Chemical Kinetics and Photochemical Data for Use in
617 Atmospheric Studies, Evaluation No. 17, JPL Publication 10-6, Jet Propulsion Laboratory, Pasadena, 2011,
618 (<http://jpldataeval.jpl.nasa.gov>; last access 15 June 2018), 2011.
- 619 Sioris, C. E., McLinden, C. A., Fioletov, V. E., Adams, C., Zawodny, J. M., Bourassa, A. E., Roth, C. Z., and
620 Degenstein, D. A.: Trend and variability in ozone in the tropical lower stratosphere over 2.5 solar cycles observed
621 by SAGE II and OSIRIS, Atmos. Chem. Phys., 14, 3479-3496, [doi: 10.5194/acp-14-3479-2014](https://doi.org/10.5194/acp-14-3479-2014), 2014.
- 622 Søvde, O. A., Prather, M. J., Isaksen, I. S. A., Berntsen, T. K., Stordal, F., Zhu, X., Holmes, C. D., and Hsu, J.: The
623 chemical transport model Oslo CTM3, Geosci. Model Dev., 5, 1441–1469, [doi: 10.5194/gmd-5-1441-2012](https://doi.org/10.5194/gmd-5-1441-2012), 2012.
- 624 Steinbrecht, W., Claude, H., Köhler, U., and Hoinka, K. P.: Correlations between tropopause height and total ozone:
625 Implications for long-term changes, J. Geophys. Res., 103 (D15), 19183-19192, 1998.

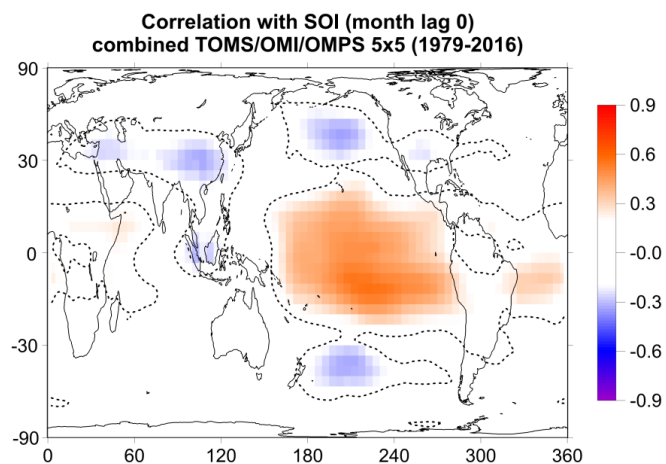


- 626 Steinbrecht, W., Claude, H., Köhler, U., and Winkler, P.: Interannual changes of total ozone and Northern
627 Hemisphere circulation patterns, *Geophys. Res. Lett.*, 28, 1191-1194, 2001.
- 628 Steinbrecht, W., Köhler, U., Claude, H., Weber, M., Burrows, J. P., and van der A, R. J.: Very high ozone columns
629 at northern mid-latitudes in 2010, *Geophys. Res. Lett.*, 38 (6), L06803, doi: 10.1029/2010GL046634, 2011.
- 630 Tourpali, K., Zerefos, C. S., Balis, D. S., and Bais, A. F.: The 11-year solar cycle in stratospheric ozone:
631 Comparison between Umkehr and SBUVv8 and effects on surface erythemal irradiance, *J. Geophys. Res.*, 112
632 (D12), D12306, doi: 10.1029/2006JD007760, 2007.
- 633 Van Roozendael, M., Spurr, R. J. D., Loyola, D., Lerot, C., Balis, D. S., Lambert, J.C., Zimmer, W., van Gent, J.,
634 van Geffen, J., Koukouli, M., Doicu, A., and Zehner, C.: Sixteen years of GOME/ERS-2 total ozone data: The new
635 direct-fitting GOME Data Processor (GDP) version 5 – Algorithm description, *J. Geophys Res.*, 117, D03305, doi:
636 10.1029/2011JD016471, 2012.
- 637 WMO (World Meteorological Organization), *Scientific Assessment of Ozone Depletion: 2014*, Global Ozone
638 Research and Monitoring Project–Report No. 55, 416 pp., Geneva, Switzerland, 2014.
- 639 Zerefos, C. S.: On the quasi-biennial oscillation in stratospheric temperatures and total ozone, *Advances in Space*
640 *Research*, 2, 177–181, 1983.
- 641 Zerefos, C. S., Bais, A. F., and Ziomas, I. C.: On the Relative Importance of Quasi-Biennial Oscillation and El
642 Nino/Southern Oscillation in the Revised Dobson Total Ozone Records, *J. Geophys. Res.*, 97 (D9), 10135–10144,
643 1992.
- 644 Zerefos, C., Contopoulos, G., and G. Skalkeas G. (Eds.): *Twenty Years of Ozone Decline*, Proceedings of the
645 Symposium for the 20th Anniversary of the Montreal Protocol, Springer, Netherlands, Part of Springer Science +
646 Business Media B. V, 470 pp., ISBN: 978-90-481-2468-8, 2009.
- 647 Zerefos, C. S., Tourpali, K., and Bais, A. F.: Further studies on possible volcanic signal to the ozone layer, *J.*
648 *Geophys. Res.*, 99 (D12), 25741–25746, 1994.
- 649 Zerefos, C. S., Tourpali, K., Isaksen, I. S. A., and Schuurmans, C. J. E.: Long term solar induced variation in total
650 ozone, stratospheric temperatures and the tropopause, *Adv. Space Res.*, 27 (12), 1943–1948, 2001.
- 651
- 652



653 **Appendix A**

654

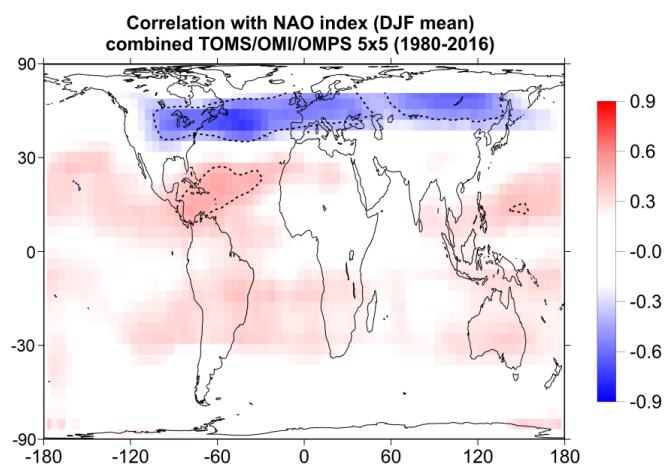


655

656

657 **Figure A1. Map of correlation coefficients between total ozone from TOMS/OMI/OMPS satellite data and**
658 **SOI for the whole period 1979-2016, after removing variability related to the seasonal cycle and the QBO.**
659 **The dotted line bounds the regions where the correlation coefficients are statistically significant at the 99%**
660 **confidence level (t-test).**

661



662

663

664 **Figure A2. Map of correlation coefficients between total ozone from TOMS/OMI/OMPS satellite data and the**
665 **NAO index in winter (DJF mean) for the whole period 1980-2016, after removing variability related to the**
666 **seasonal cycle and the QBO. The dotted line bounds the regions where the correlation coefficients are**
667 **statistically significant at the 99% confidence level (t-test).**

668

669



670

671 **Table 1. Mean differences and their standard deviations in percent between total ozone from GOME-2A,**
 672 **SBUV (v8.6) satellite overpass data and ground-based observations over different latitude zones, as shown in**
 673 **Figures 1 and 2.**

674

| | [GOME-2A – SBUV] / SBUV (%) Stations mean data | [GOME-2A – GROUND] / GROUND (%) Stations mean data |
|-----------|---|---|
| 60°-80° N | +1.3 ± 2.2 | +2.5 ± 3.2 |
| 30°-60° N | +0.8 ± 1.6 | +0.1 ± 1.9 |
| 0°-30° N | 0.0 ± 0.7 | -0.5 ± 1.2 |
| 0°-30° S | +0.1 ± 0.7 | -0.9 ± 1.6 |
| 30°-60° S | +0.9 ± 1.6 | 0.0 ± 2.4 |
| 60°-80° S | -0.5 ± 2.9 | 0.0 ± 4.3 |

675

676

677 **Table 2. Mean differences and their standard deviations in percent between deseasonalised total ozone data**
 678 **from GOME-2A, SBUV (v8.6) satellite overpass data and ground-based observations over different latitude**
 679 **zones, as shown in Figures 5 and 6.**

680

| | [GOME-2A – SBUV] (%) Stations mean deseasonalized data | [GOME-2A – GROUND] (%) Stations mean deseasonalized data |
|-------------|---|---|
| 30°-60° N | -0.1 ± 0.7 | -0.1 ± 0.9 |
| 10°-30° N | -0.3 ± 0.5 | -0.8 ± 0.8 |
| 10° N-10° S | +0.1 ± 0.6 | +0.1 ± 1.0 |
| 10°-30° S | 0.0 ± 0.7 | -0.1 ± 0.9 |
| 30°-60° S | -0.1 ± 1.0 | -0.4 ± 1.0 |

681

682



683

684 **Table 3. Annual mean total ozone, amplitude of annual cycle, amplitude of QBO and amplitude of ENSO in the period 1995-2016 from GTO-ECV, the**
 685 **combined TOMS/OMI/OMPS satellite data and Oslo CTM3 model calculations over the South Pacific region (10°-20° S, 180°-220° E) and at station**
 686 **Samoa (14.25° S, 189.4° E) located within this region.**

687

| | South Pacific Ocean | | | station Samoa | | |
|---------------------------|---------------------|---------------|---------------|---------------|---------------|---------------|
| | GTO-ECV | TOMS/OMI/OMPS | Oslo CTM3 | GTO-ECV | GROUND | SBUV |
| Annual mean | 254.7 DU | 253.0 DU | 259.5 DU | 252.2 DU | 249.2 DU | 251.9 DU |
| Amplitude of annual cycle | 7.7 DU (3.0%) | 7.3 DU (2.9%) | 5.2 DU (2.0%) | 6.7 DU (2.7%) | 6.7 DU (2.7%) | 7.3 DU (2.9%) |
| Amplitude of QBO | 2.2 DU (0.9%) | 2.4 DU (0.9%) | 2.3 DU (0.9%) | 2.2 DU (0.9%) | 2.7 DU (1.1%) | 2.0 DU (0.8%) |
| Amplitude of ENSO | 8.7 DU (3.4%) | 6.0 DU (2.4%) | 8.9 DU (3.4%) | 7.6 DU (3.0%) | 5.7 DU (2.3%) | 7.6 DU (3.0%) |

688

689



690

691 **Table 4. Annual mean total ozone, amplitude of annual cycle, amplitude of QBO and amplitude of NAO in the period 1995-2016 from GTO-ECV, the**
 692 **combined TOMS/OMI/OMPS satellite data and Oslo CTM3 model calculations over the North Atlantic Ocean: (a) region 35°-50° N, 20°-50° W, and (b)**
 693 **region 15°-27° N, 30°-60° W.**

694

| | North Atlantic Ocean | | | | | |
|---------------------------|--------------------------|-----------------|-----------------|--------------------------|----------------|----------------|
| | (a) 35°-50° N, 20°-50° W | | | (b) 15°-27° N, 30°-60° W | | |
| | GTO-ECV | TOMS/OMI/OMPS | Oslo CTM3 | GTO-ECV | TOMS/OMI/OMPS | Oslo CTM3 |
| Annual mean | 315.9 DU | 317.3 DU | 311.2 DU | 276.4 DU | 274.4 DU | 282.6 DU |
| Amplitude of annual cycle | 37.0 DU (11.7%) | 36.9 DU (11.6%) | 32.0 DU (10.3%) | 15.8 DU (5.7%) | 15.1 DU (5.5%) | 15.5 DU (5.5%) |
| Amplitude of QBO | 2.3 DU (0.7%) | 2.6 DU (0.8%) | 3.2 DU (1.0%) | 2.8 DU (1.0%) | 3.9 DU (1.4%) | 4.3 DU (1.5%) |
| Amplitude of NAO (winter) | 18.3 DU (5.8%) | 17.5 DU (5.5%) | 20.3 DU (6.5%) | 8.8 DU (3.2%) | 7.2 DU (2.6%) | 8.0 DU (2.8%) |

695

696



697

698 **Table 5. Annual mean total ozone, amplitude of annual cycle, amplitude of QBO and amplitude of NAO in the period 1995-2016 from GTO-ECV**
 699 **satellite data, ground-based observations and SBUV (v8.6) satellite overpass data over: (a) Canada and USA (11 stations mean), and (b) Europe (41**
 700 **stations mean).**

701

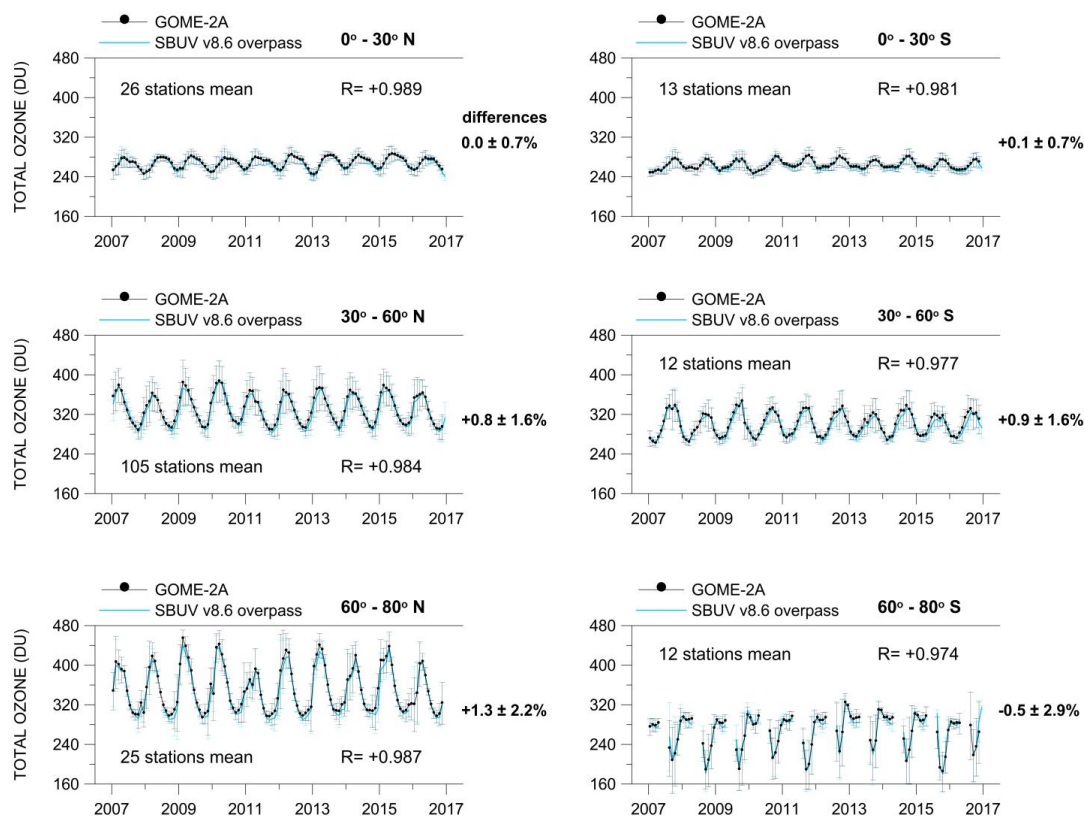
| | (a) Canada and USA | | | (b) Europe | | |
|---------------------------|--|-----------------|-----------------|---|-----------------|-----------------|
| | 30°-50° N, 60°-110° W (11 stations mean) | | | 35°-55° N, 10° W-40° E (41 stations mean) | | |
| | GTO-ECV | GROUND | SBUV | GTO-ECV | GROUND | SBUV |
| Annual mean | 320.6 DU | 322.5 DU | 320.9 DU | 325.7 DU | 326.9 DU | 326.8 DU |
| Amplitude of annual cycle | 34.1 DU (10.6%) | 33.2 DU (10.3%) | 34.0 DU (10.6%) | 40.5 DU (12.4%) | 39.2 DU (12.0%) | 40.7 DU (12.4%) |
| Amplitude of QBO | 2.5 DU (0.8%) | 3.5 DU (1.1%) | 2.6 DU (0.8%) | 1.9 DU (0.6%) | 2.8 DU (0.8%) | 2.2 DU (0.7%) |
| Amplitude of NAO (winter) | 9.5 DU (3.0%) | 10.2 DU (3.2%) | 11.1 DU (3.5%) | 12.7 DU (3.9%) | 16.5 DU (5.1%) | 14.7 DU (4.5%) |

702

703



704



705

706

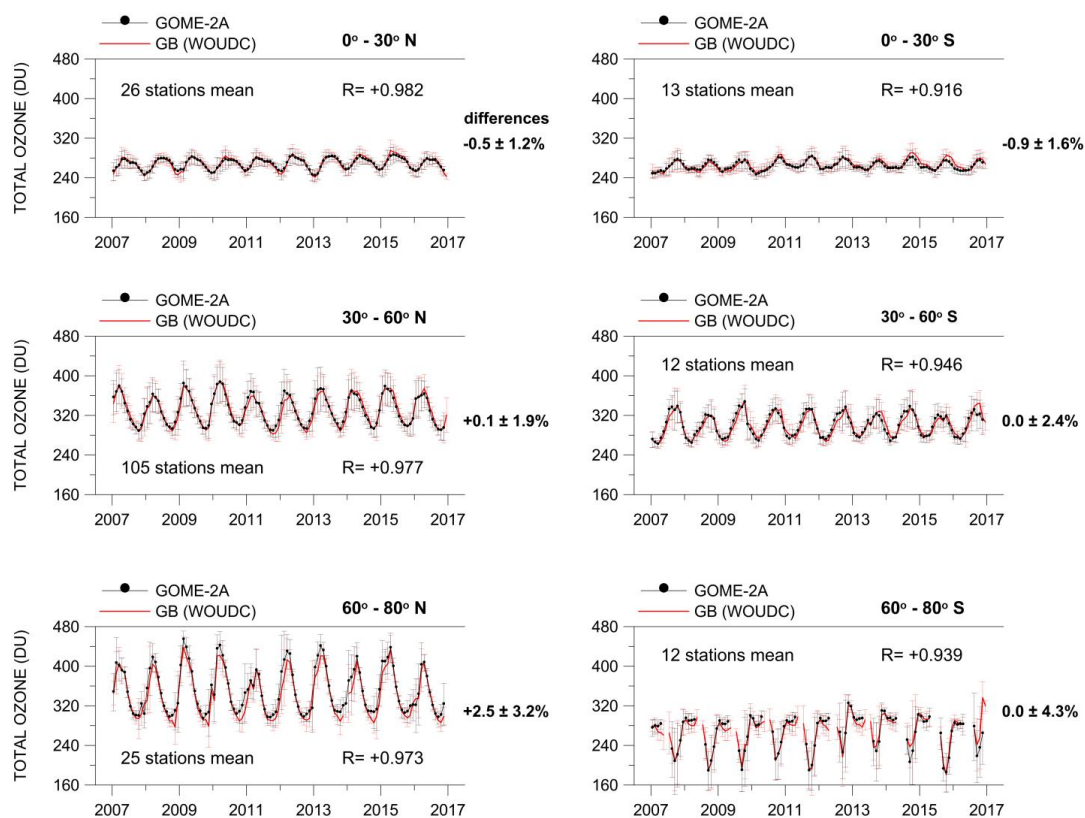
707 **Figure 1. Monthly mean total ozone from GOME-2A as compared with monthly mean total ozone from**
 708 **SBUV (v8.6) satellite overpass data for the period 2007-2016 over the Northern and the Southern Hemisphere**
 709 **based on stations mean data. R is the correlation coefficient between the two lines. Error bars show the**
 710 **standard deviation of each monthly mean. Mean differences ± σ are given as [GOME-2A – SBUV] / SBUV**
 711 **(%).**

712

713



714



715

716

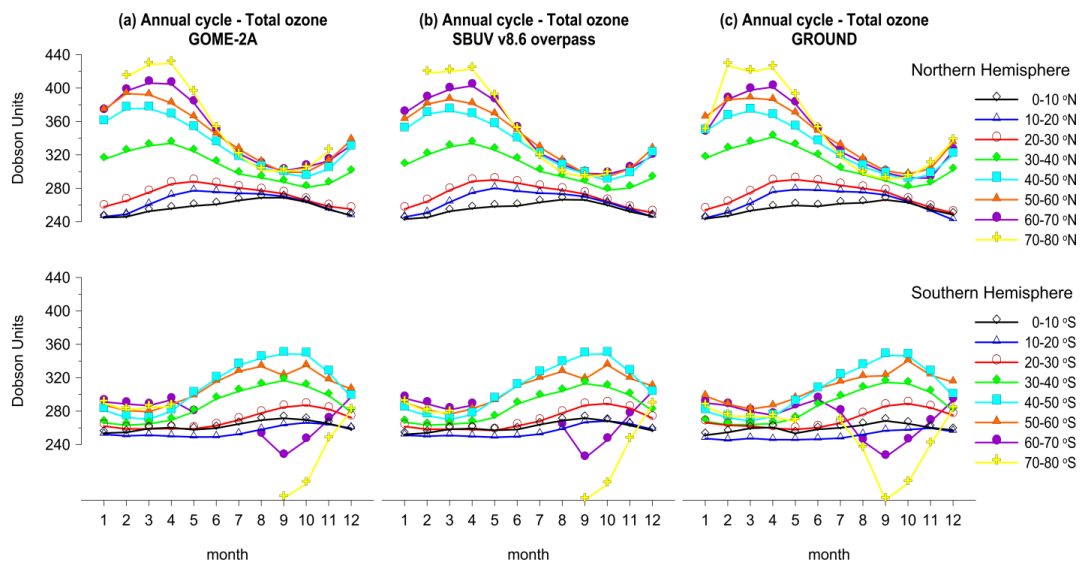
717 **Figure 2. Same as in Figure 1 but for GOME-2A and GB observations. *R* is the correlation coefficient**
 718 **between the two lines. Error bars show the standard deviation of each monthly mean. Mean differences ± σ**
 719 **are given as [GOME-2A – GROUND] / GROUND (%).**

720

721



722



723

724

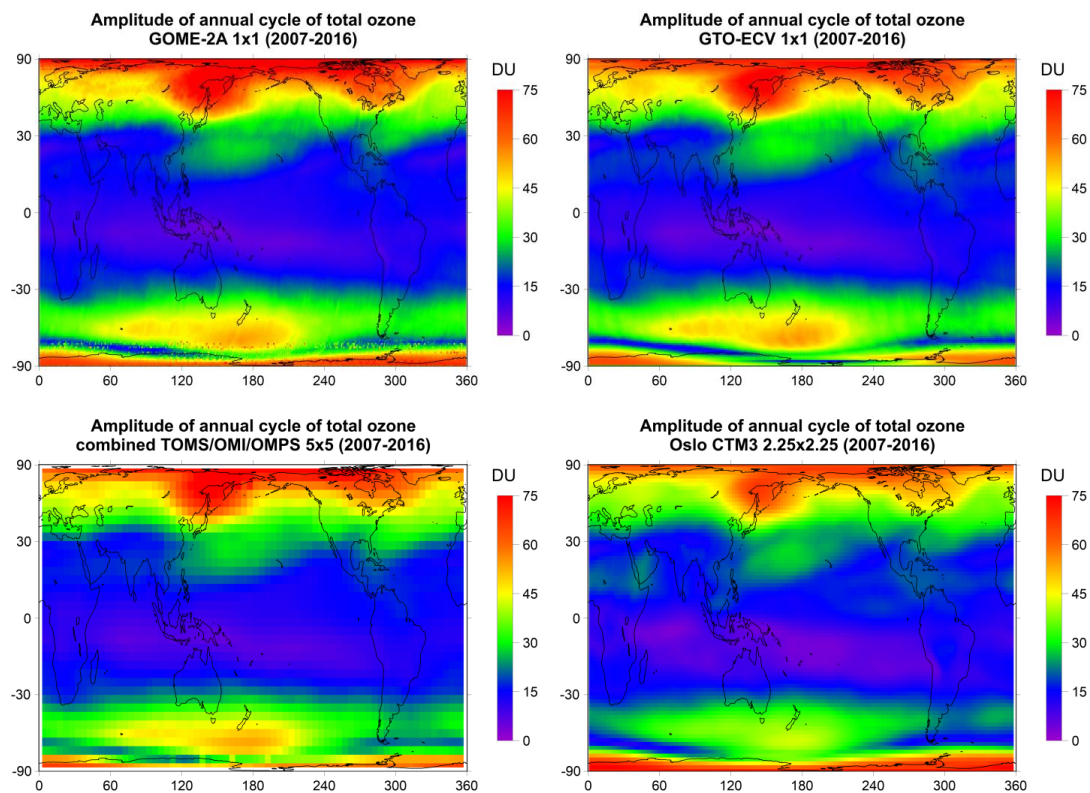
725 **Figure 3. Comparison of the annual cycle of total ozone from GOME-2A with that from SBUV (v8.6) satellite**
726 **overpass data and GB observations in the period 2007-2016 based on stations data averaged per 10 degree**
727 **latitude zones. The annual cycle is distorted above 60 deg. S due to the Antarctic ozone hole.**

728

729



730



731

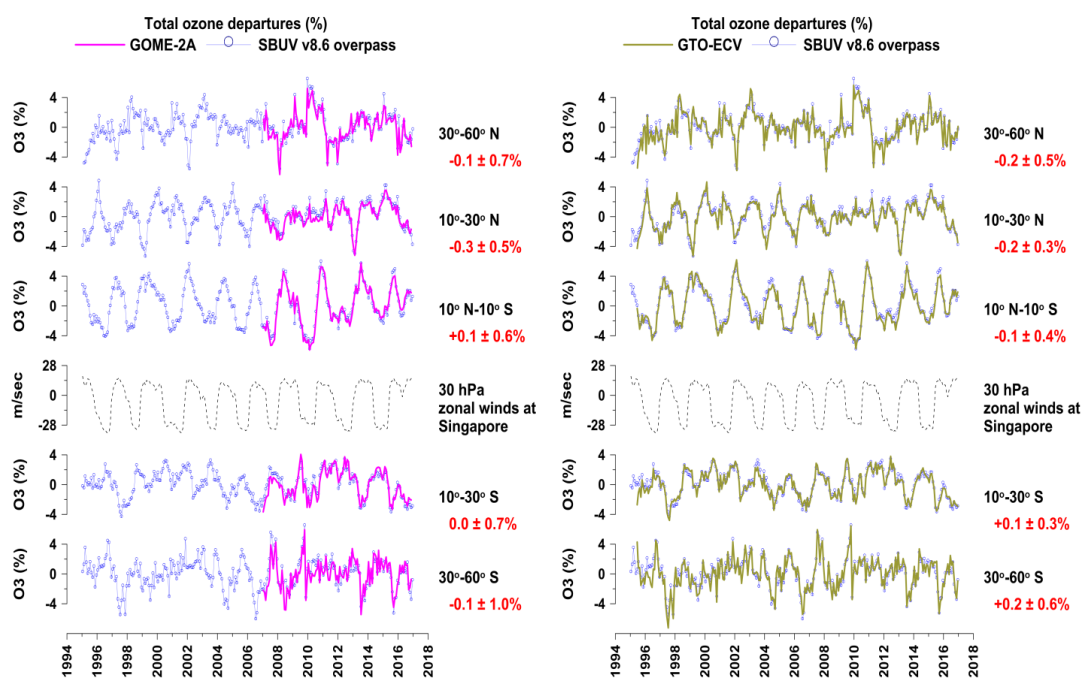
732 **Figure 4. Comparison of the amplitude [i.e., (max-min)/2] of the annual cycle of total ozone from GOME-2A**
733 **(upper left) with the amplitude of the annual cycle of total ozone from GTO-ECV (upper right), the combined**
734 **TOMS/OMI/OMPS satellite data (lower left) and Oslo CTM3 model simulations (lower right).**

735

736



737



738

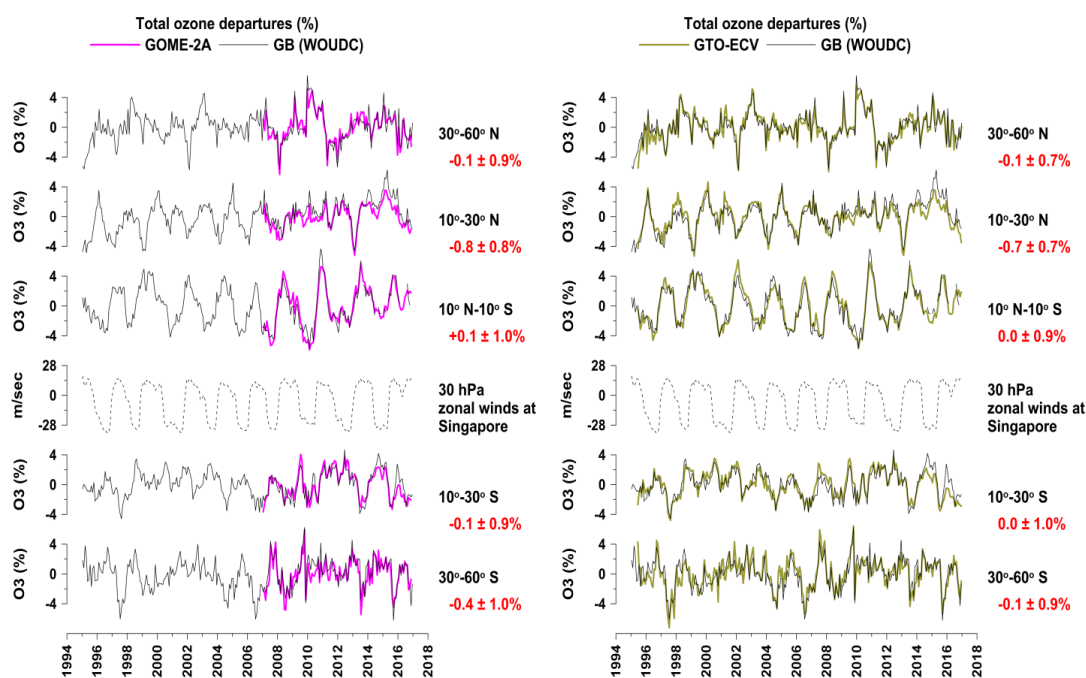
739 **Figure 5. (Left panel) Time series of deseasonalised total ozone from GOME-2A and SBUV (v8.6) satellite**
 740 **overpasses over different latitude zones along with the equatorial zonal winds at 30 hPa as an index of the**
 741 **QBO; (Right panel) same as in left panel but for GTO-ECV and SBUV. Values with red colour refer to the**
 742 **mean differences $\pm \sigma$ (in %) between GOME-2A and SBUV deseasonalised data averaged over various**
 743 **WOUDC stations (150 stations in the northern mid-latitudes (30°-60° N), 21 stations in the northern**
 744 **subtropics (10°-30° N), 8 stations in the tropics (10° S-10° N), 10 stations in southern subtropics (10°-30° S) and**
 745 **12 stations in the southern mid-latitudes (30°-60° S)).**

746

747



748



749

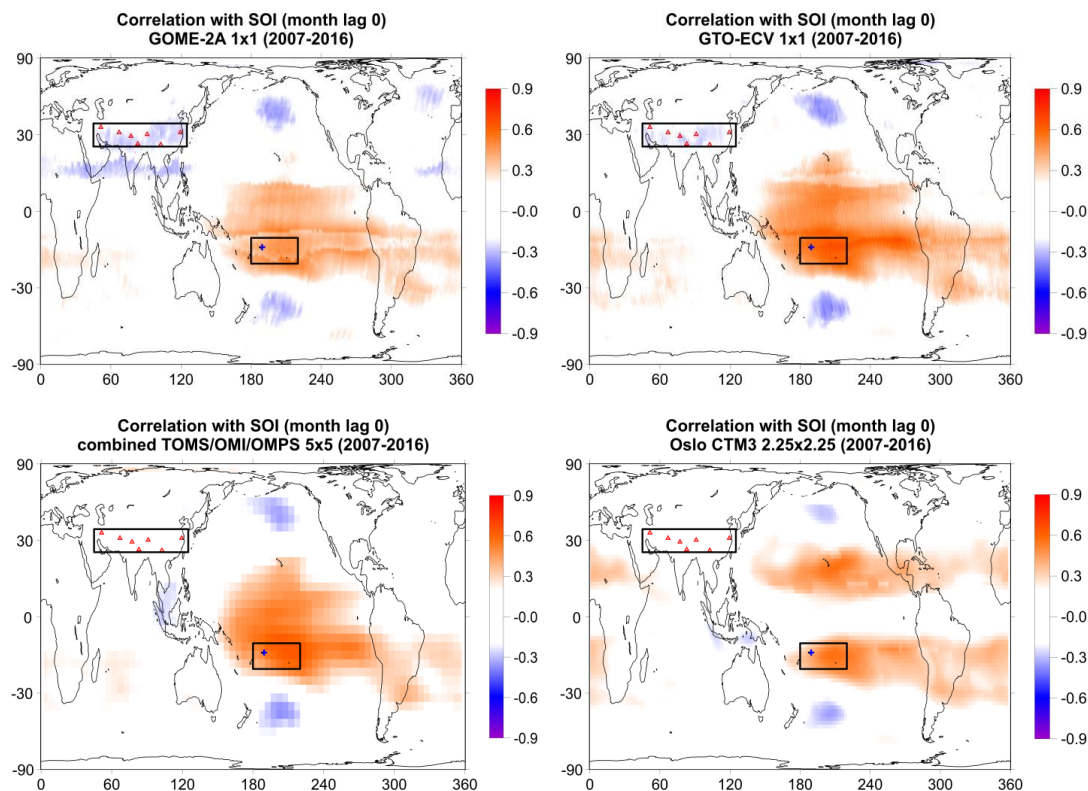
750 **Figure 6.** Same as in Figure 5 but for GOME-2A and GB observations (left panel), and for GTO-ECV and
 751 GB observations (right panel).

752

753



754

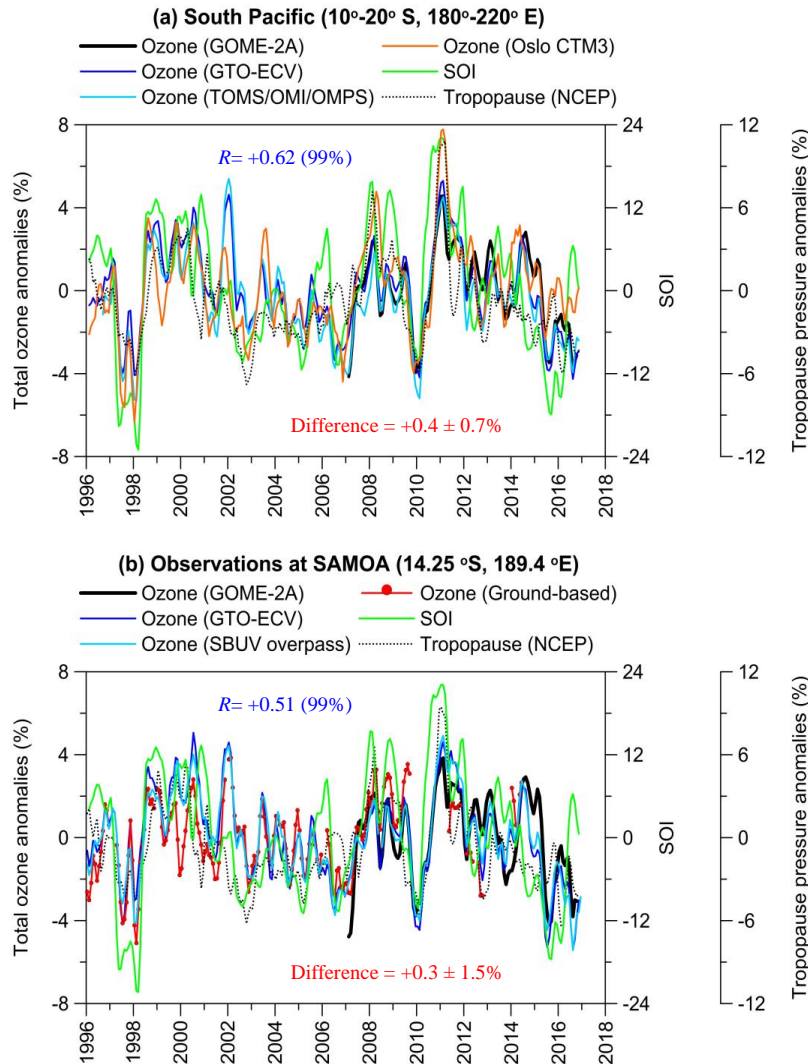


755

756 **Figure 7.** Map of correlation coefficients between total ozone and SOI for GOME-2A (upper left), GTO-ECV
757 (upper right), TOMS/OMI/OMPS satellite data (lower left) and Oslo CTM3 model simulations (lower right).
758 Rectangles correspond to the South Pacific region (10-20 °S, 180-220 °E) and South Asia region (35-45 °N, 45-
759 125 °E), blue cross to the station Samoa (14.25 °S, 189.4 °E) and red triangles to stations in South Asia, in
760 which total ozone has been studied as for the impact of ENSO after removing variability related to the annual
761 cycle and the QBO. Positive correlations are shown by red colours while negative correlations by blue
762 colours. Only correlation coefficients above/below ± 0.2 are shown.

763

764

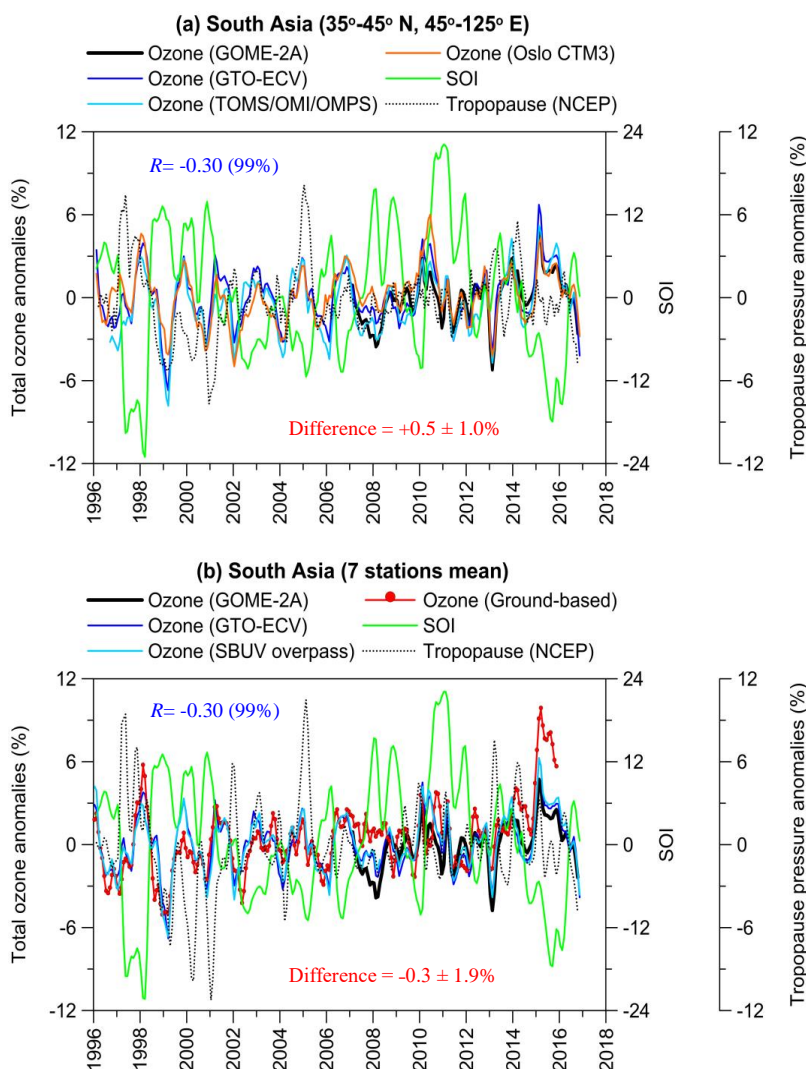


765

766 **Figure 8. (a) Example of regional time series of total ozone (%) over the South Pacific region (10°-20° N, 180°-**
 767 **220° E) along with SOI. The dotted line shows the respective tropopause pressure variability from NCEP. R is**
 768 **the correlation coefficient between GTO-ECV total ozone and SOI (statistical significance of R is given in**
 769 **parentheses). The difference refers to the mean difference $\pm \sigma$ (in %) between GTO-ECV and the combined**
 770 **TOMS/OMI/OMPS satellite data. (b) Same as in (a) but for SBUV overpass and GB data at the station**
 771 **Samoa. The difference refers to the mean difference $\pm \sigma$ (in %) between GTO-ECV and GB data.**

772

773



774

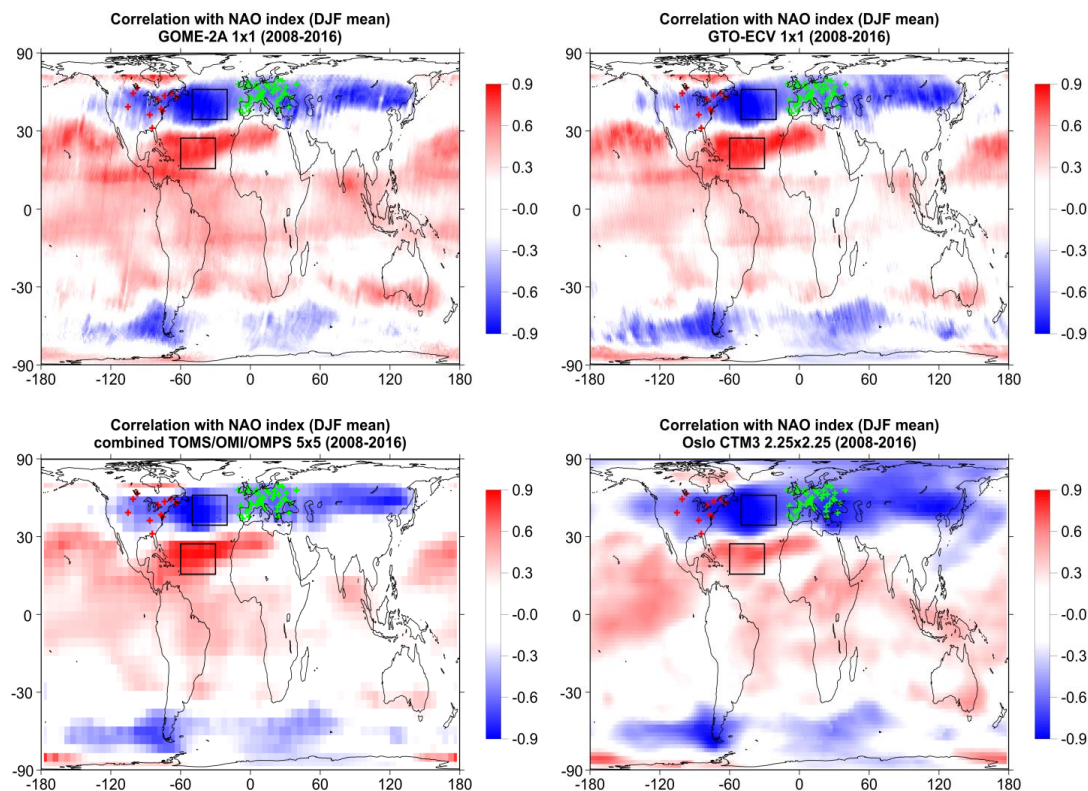
775 **Figure 9. (a) Example of regional time series of total ozone (%) over South Asia (35°-45° N, 45°-125° E) along**
 776 **with SOI. The dotted line shows the respective tropopause pressure variability from NCEP. R is the**
 777 **correlation coefficient between GTO-ECV total ozone and SOI (statistical significance of R is given in**
 778 **parentheses). The difference refers to the mean difference $\pm \sigma$ (in %) between GTO-ECV and the combined**
 779 **TOMS/OMI/OMPS satellite data. (b) Same as in (a) but with SBUV overpass and GB data averaged at 7**
 780 **stations in South Asia. The difference refers to the mean difference $\pm \sigma$ (in %) between GTO-ECV and GB**
 781 **data.**

782

783



784



785

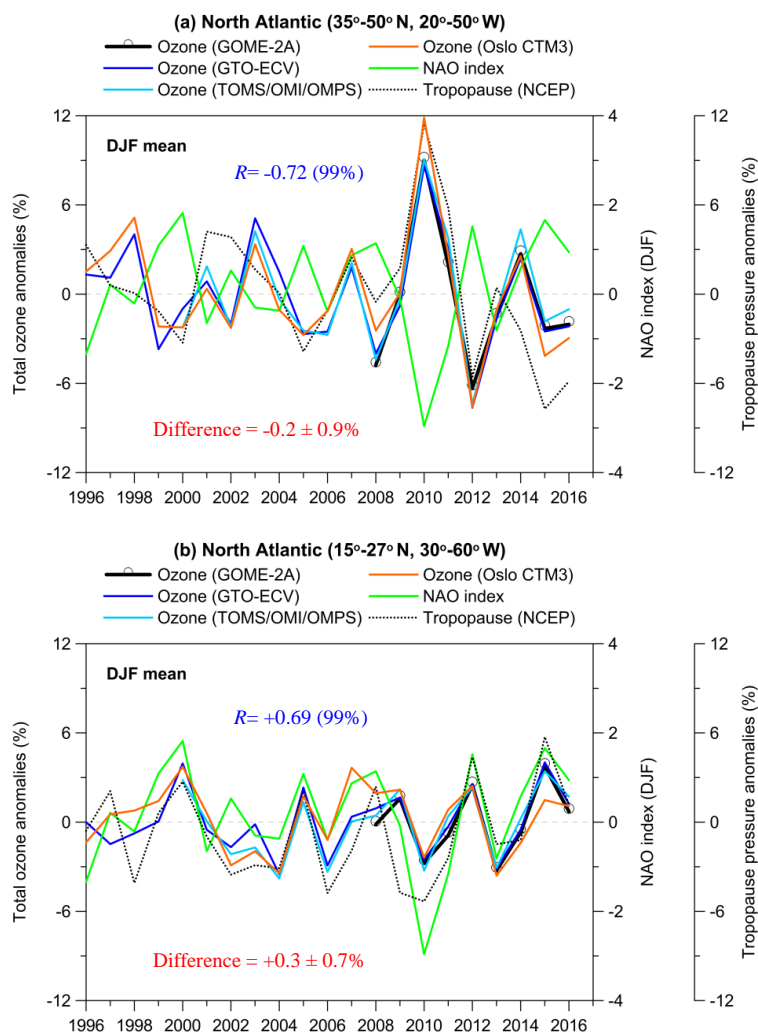
786 **Figure 10. Map of correlation coefficients between total ozone and the NAO index in winter (DJF mean) for**
787 **GOME-2A (upper left), GTO-ECV (upper right), TOMS/OMI/OMPS satellite data (lower left) and Oslo**
788 **CTM3 model simulations (lower right). Rectangles correspond to regions in the North Atlantic (35°-50° N,**
789 **20°-50° W; 15°-27° N, 30°-60° W), and red and green crosses to stations in Canada/USA and Europe, in which**
790 **total ozone has been studied as for the impact of NAO after removing variability related to the annual cycle**
791 **and the QBO. Positive correlations are shown by red colours while negative correlations by blue colours.**
792 **Only correlation coefficients above/below ± 0.2 are shown.**

793

794



795



796

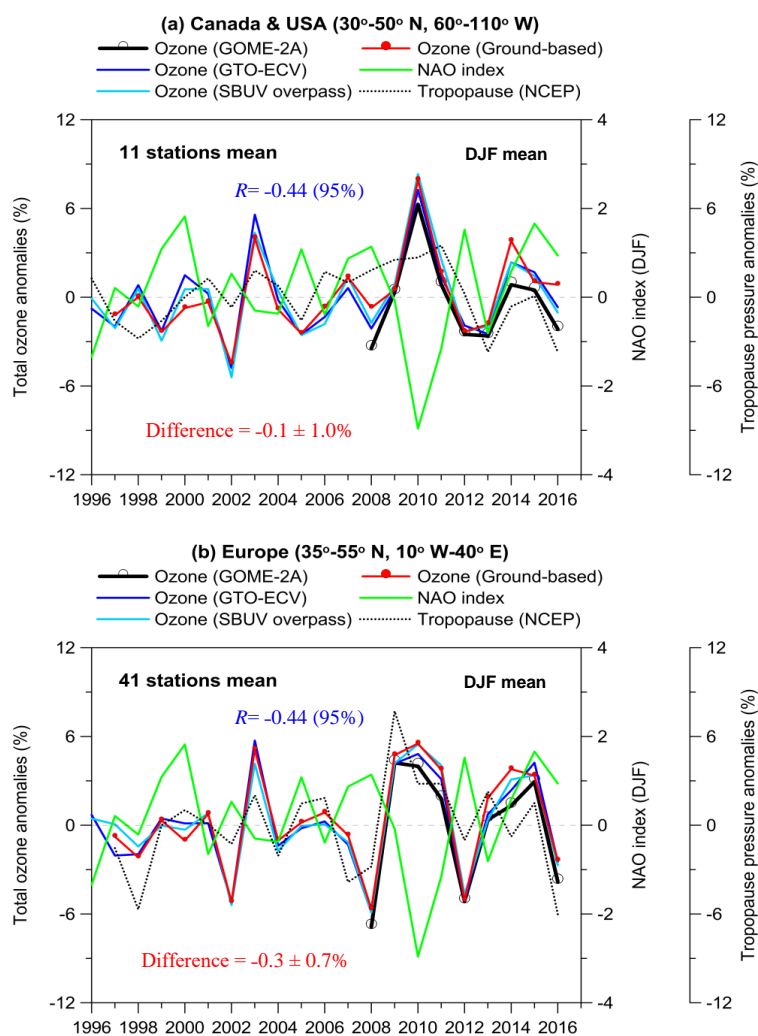
797 **Figure 11.** Example of regional time series of total ozone (%) over the North Atlantic regions (a) 35°-50° N,
 798 20°-50° W and (b) 15°-27° N, 30°-60° W in winter (DJF mean) along with the NAO index. The dotted line
 799 shows the respective tropopause pressure variability from NCEP reanalysis. R is the correlation coefficient
 800 between GTO-ECV total ozone and the NAO index. The differences refer to the mean differences $\pm \sigma$ (in %)
 801 between GTO-ECV and the combined TOMS/OMI/OMPS satellite data.

802

803



804



805

806 **Figure 12.** Comparison with GB observations over: (a) Canada and USA and (b) Europe in winter (DJF
 807 mean). R is the correlation coefficient between GTO-ECV total ozone and the NAO index. The differences
 808 refer to the mean differences $\pm \sigma$ (in %) between GTO-ECV and GB data.

809